

1 **Evolution of clay mineral assemblages in the Tinguiririca**  
2 **geothermal field, Andean Cordillera of central Chile: An XRD and**  
3 **HRTEM-AEM study**

4  
5 **M. Vázquez<sup>1\*</sup>, F. Nieto<sup>2</sup>, D. Morata<sup>1</sup>, B. Droguet<sup>1,3,4</sup>, F.J. Carrillo-Rosua<sup>2,5</sup>, S.**  
6 **Morales<sup>2</sup>**

7  
8 **1. Department of Geology and Andean Geothermal Center of Excellence**  
9 **(CEGA), Facultad de Ciencias Físicas y Matemáticas, Universidad de Chile,**  
10 **Plaza Ercilla 803, Santiago, Chile**

11  
12 **2. Departamento de Mineralogía y Petrología and Instituto Andaluz de**  
13 **Ciencias de la Tierra, Universidad de Granada-CSIC. Avenida Fuentenueva,**  
14 **18002. Granada, Spain**

15  
16 **3. Energía Andina S.A, Cerro El Plomo 5630, Santiago, Chile.**

17 **4. Current address: Amawta consultores. Almirante Pastene 185, Santiago,**  
18 **Chile**

19  
20 **5. Departamento de Didáctica de las Ciencias Experimentales, Universidad**  
21 **de Granada. Campus Cartuja, 18071. Granada, Spain**

22  
23  
24 **Abstract**

25 HRTEM textural evidence shows that clay minerals in the Tinguiririca geothermal  
26 field (Andean Cordillera, central Chile) are the result of direct alteration of former  
27 volcanic glass and minerals by hydrothermal fluids at similar temperatures to the  
28 present day. They show the classical pattern of diagenetic transformation from

---

\* Corresponding author. Tel.: +56-2-29784539; #Fax: +56-2-26963050  
E-mail address: [mvazquez@ing.uchile.cl](mailto:mvazquez@ing.uchile.cl) (M.Vázquez)

1 smectite at the top to illite at the bottom, with the progressive formation of  
2 corrensite and chlorite. The high fluid/rock ratio, disposability of necessary  
3 cations and absence of previous detrital phyllosilicates allow the consideration of  
4 this area as a natural laboratory to establish the extreme ideal conditions for very  
5 low-T reactions. Transformations from smectite to R1 illite-smectite (I-S) and from  
6 these to R3 mixed-layers occur respectively at 80-120°C and 125-180°C. In spite  
7 of ideal genetic conditions, the new-formed minerals show all the defective  
8 character and lack of textural and chemical equilibrium previously described in  
9 the literature for diagenetic and hydrothermal low-temperature assemblages.  
10 Chemistry of smectite-illite phases evolves basically through a diminution of the  
11 pyrophyllitic component toward a theoretical muscovite ( $\text{Si}^{4+} + \square \rightarrow \text{Al}^{3+} + \text{K}^+$ ).  
12 However, a second chemical vector ( $\text{Si}^{4+} + \text{Mg}^{2+} \rightarrow \text{Al}^{3+} + \text{Al}^{3+}$ ), that is, decreasing  
13 of the tschermack component, also contributes to the evolution toward the less  
14 Si-more Al rich muscovite in relation to the original smectite. Residual Mg (and  
15 Fe) from the latter reaction is consumed in the genesis of chloritic phases.  
16 Nevertheless, as a consequence of the lack of chemical equilibrium (probably  
17 because of the short time-scale of the geothermal alteration processes), the  
18 composition of clay minerals is highly heterogeneous at the level of a single  
19 sample. Consequently, the respective fields of smectite, R1 I-S and R3 I-S  
20 overlap each other, making the distinction among these three phases impossible  
21 based exclusively on chemical data.

22

23 *Keywords: geothermal alteration, clay minerals, reaction progress, XRD,*  
24 *HRTEM-AEM, Andean Cordillera, Chile.*

25

## 26 **1. Introduction**

27 A progressive series of clay mineral reactions occurs during diagenesis; these  
28 reactions increase the sediment density and reduce pore-space as new, bedding-  
29 parallel authigenic phyllosilicates invade and fill voids (Merriman and Peacor,  
30 1999). Most clay minerals progressively change from random-oriented to a more  
31 or less oriented fabric when the conditions of low-temperature metamorphism are

1 attained. The physical, mineralogical and chemical modifications exhibited by  
2 phyllosilicates during diagenesis are widely applied in petroleum exploration,  
3 allowing the identification of the necessary conditions for the transition from dry-  
4 gas phase to unproductive rocks, which occurs during the evolution from deep  
5 diagenesis to anchizone.

6  
7 During low-temperature processes, thermodynamic equilibrium is not attained by  
8 the paragenesis of clay minerals (Merriman et al., 1995; Árkai et al., 1996, 2000;  
9 Warr and Nieto, 1998; Abad et al., 2001, 2003a, b). The mineralogical  
10 transformations are controlled, in addition to temperature and pressure, by other  
11 additional factors such as the original material and the chemical composition,  
12 time, fluid/rock ratio and tectonic stress. Consequently, the crystal-chemical  
13 parameters of phyllosilicates cannot be used for geothermometric  
14 determinations. The clay mineral reactions are governed by the Ostwald Step  
15 Rule (Morse and Casey, 1988), which states that the clay mineral paragenesis  
16 evolves through the formation of successive metastable phyllosilicates, that  
17 progress towards the state of stable chemical and textural equilibrium (eg. Nieto  
18 et al. 1996). This is reached during greenschist-facies (Abad et al., 2006).  
19 However, the characteristics of clay minerals are qualitative indicators of the  
20 reaction progress, in other words, the stage which phyllosilicates have reached  
21 through a series of metastable mineral reactions (Merriman and Peacor, 1999).

22  
23 A plethora of researchers have studied clay minerals in low-temperature  
24 processes. Nevertheless, no agreement exists about the temperature for the  
25 various mineral changes or the mineral genesis mechanism. Smectite illitization  
26 and the formation of chlorite are the processes most often referred to in the  
27 literature. Smectite illitization onset is marked by the disappearance of smectite  
28 or R0 illite-smectite mixed-layers (hereafter, I-S) and the formation of R1 I-S. This  
29 occurs at temperatures from 75 to 120° C (Hoffman and Hower, 1979; Srdonon  
30 and Eberl, 1984; Schegg and Leu, 1996; Usysal et al., 2000; Adid et al., 2004).  
31 The transition from R1 to R3- ordered I-S occurs up to 175° C (Hoffman and

1 Hower 1979; Weaver 1989; Lindgreen 1991; Pollastro 1993, Abid et al., 2004).  
2 However, the temperature of this mineralogical change could be higher and  
3 depends on the characteristics of the original materials (eg. Arostegui et al.,  
4 2006). Additionally, illitization can be inhibited in sediments with low K contents  
5 and low porosity and/or in sediments with high Mg and Ca contents. On the other  
6 hand, the temperature of chlorite formation is between 100 and 270° C, broadly  
7 coinciding with the development of I-S.

8

9 Hydrothermal systems offer a simpler scenario for the study of low-T processes  
10 under a more constrained set of parameters. The presence of a sufficient hot  
11 fluid phase in these hydrothermal systems compared with restricted and limited  
12 water availability in diagenetic transformations during burial would imply a higher  
13 fluid/rock ratio that could guarantee a more rapid and complete evolution and, in  
14 part, liberates the system from the influence of the original material. Clay  
15 minerals are widespread alteration products in most active and fossil geothermal  
16 systems, being excellent tracers of their hydrothermal history (e.g. Mas et al.,  
17 2003, 2006 and references therein). Many studies have considered both the  
18 sequential distribution from smectites to non-expandable di- or trioctahedral  
19 phyllosilicates and the chemical variations of the non-expandable clay phases  
20 (e.g. chlorite and/or illite) as a function of past or present thermal conditions (e.g.  
21 Cathelineau and Nieva, 1985; Ji and Browne, 2000). However, properties of clay  
22 minerals are not only affected by temperature but also by rock and fluid  
23 chemistry, time, fluid/rock ratio, the nature of the precursor material or  
24 mechanism of crystal growth (e.g. Essene and Peacor, 1995; López Munguira et  
25 al., 2002). These factors affect the structure (coherent domain size in the c-  
26 direction, polytypism, mixed-layering), composition (cation site occupancy) and  
27 texture (particle size, morphology). Consequently, the conditions at which these  
28 minerals crystallized in the active and fossil geothermal fields are more properly  
29 approached by an integrated study of all the crystal parameters of clay minerals  
30 at the field scale.

31

1 The Salton Sea geothermal field in southeastern California has long been of  
2 interest to geologists as an area of hydrothermal metamorphism of detrital  
3 sediments, from diagenesis to greenschist facies, with a continuous progression  
4 of minerals as a function of depth (Muffler & White, 1969). White mica, chlorite  
5 and biotite were found to change gradually from the initial fine-grained materials  
6 to coarser-grained, more mature crystals, suggesting continued growth of  
7 crystals with burial, as consistent with the concept of burial metamorphism. Yau  
8 et al. (1987a,b, 1988) utilized transmission, analytical and scanning electron  
9 microscopy (TEM, AEM, SEM) to characterize the minerals and the processes of  
10 transformation. They described three phyllosilicate zones: (1) illite-muscovite  
11 (115 –220°C), (2) chlorite (220 –310°C), (3) biotite (>310°C). Giorgetti et al.  
12 (2000) showed that in the shallowest parts of this geothermal field the detrital  
13 kaolinite and muscovite reacted to form interstratified illite-smectite (I-S), which in  
14 turn was replaced by illite. The textures and microstructures observed indicate  
15 that the mineral progression involves dissolution of original phases, mass  
16 transport through interconnecting pore space, and direct crystallization of  
17 phyllosilicates from solution (eg. Yau et al., 1988, Giorgetti et al., 2000, 2003).  
18 Phyllosilicate changes with depth were not time-dependent, because they formed  
19 simultaneously at all depths as a result of a single hydrothermal event in an open  
20 system (Giorgetti et al., 2003).

21

22 The continuous slim hole core (815 m depth) drilled in the Tinguiririca geothermal  
23 field in the Andean Cordillera of central Chile by the company Energia Andina  
24 (EASA) offers an excellent case study of clay mineral evolution in an active  
25 geothermal system. Various kinds of mixed layers, both in the smectite-illite  
26 system and the smectite-chlorite system are present, which can be correlated  
27 with the present day temperatures directly measured in the borehole and  
28 contrasted if the observed secondary mineralogy is consistent with in situ  
29 measured temperature.

30

1 The aim of this study is to determine the textural, mineral and chemical  
2 characteristics at the lattice level of the clay minerals in relation to depth in the  
3 active Tinguiririca geothermal system (Andean Cordillera of central Chile). The  
4 possibility of continuous sampling along the drill core will provide a thermal  
5 reference for the usually employed reaction progress parameters, as mineral  
6 paragenesis, type of mixed-layer and chlorite thermometry.

7

## 8 **2. Geological Setting**

9 Geothermal resources in the Andean Cordillera of Chile are spatially associated  
10 with active volcanism, which is primarily controlled by the convergence of the  
11 Nazca and South America Plates. This geological setting constraints the Chilean  
12 Andean volcanic arc as one of the largest but not yet developed geothermal  
13 areas of the world. Consequently, two main volcanic zones can be distinguished  
14 within the Chilean Andes: the Northern Volcanic Zone (17°S-28°S) and the  
15 Central-Southern Volcanic Zone (33°S-46°S) parallel to the coast.

16

17 Few studies regarding the mineralogy involved in low temperature alterations  
18 have thus far been developed in Chile (e.g. Droguet et al., 2012), with most of  
19 the published papers being focussed on fossil geothermal systems in the central  
20 Andean Cordillera (Vergara et al., 1993; Aguirre et al., 2000; Fuentes et al.,  
21 2004). The Tinguiririca Geothermal field, located only 150 km southwest of  
22 Santiago, developed on the Pleistocene-Holocene volcanic rocks of the  
23 Tinguiririca volcano (Fig. 1). The oldest geological units outcropping in the area  
24 belong to the Jurassic volcanic and volcanoclastic Rio Damas formation and the  
25 Jurassic Baños del Flaco limestone sequences. Cretaceous to Eocene-Miocene  
26 volcanic and volcanoclastic sequences overlie these sequences.. All these units  
27 were folded and thrust according to the major extensional and compressional  
28 deformation events (Clavero et al., 2011). Miocene subvolcanic stocks intrude  
29 Oligo-Miocene volcanic sequences. These deformed Meso-cenozoic units are  
30 unconformably overlain by the Lower to Upper Pleistocene Tinguiririca Volcanic  
31 Complex, mostly composed of subhorizontal calc-alkaline porphyritic basaltic to

1 andesitic lava flows with minor pyroclastic levels. Based on K/Ar whole rock  
2 dating, Arcos et al (1988) suggested two main volcanic sequences during the  
3 building of the Tinguiririca Volcanic Complex. The oldest units were developed  
4 during the Lower Pleistocene ( $1.101 \pm 0.068$  to  $0.922 \pm 0.048$  Ma), and the  
5 youngest during the Upper Pleistocene ( $0.297 \pm 0.028$  to  $0.170 \pm 0.030$  Ma). Minor  
6 Holocene post-glacial volcanic cones were also identified in this volcanic  
7 complex. Calcic plagioclase, clino and orthopyroxene and minor olivine and  
8 magnetite are the main phenocrysts within an intersectoral to hialopilitic  
9 groundmass. Three main volcanic cones (Tinguiririca, Fray Carlos and  
10 Montserrat) comprise this volcanic complex (Arcos et al., 1988). The NNE  
11 alignment of these volcanic cones is coincident with the main NNE fault system  
12 observed in the area, suggesting a strong structural control on the magmatic and  
13 also fluid paths in this section of the Andean Cordillera (Clavero et al., 2011).

14

15 Geothermal manifestations in the Tinguiririca volcanic field comprise steam  
16 vents, bubbling mud pools and flowing hot springs associated with steam-heated,  
17 acid sulfate and near neutral pH bicarbonate waters (Clavero et al., 2011). These  
18 surficial geothermal manifestations occur to the west and southwest of the  
19 Tinguiririca volcano, between 2700 and 3300 m (Fig. 1). Water and gas  
20 geochemistry together with He isotope ratios suggests equilibrium temperatures  
21 in between  $230^{\circ}$  to  $300^{\circ}\text{C}$  having He a clear magmatic source, possibly related  
22 with basaltic systems (Clavero et al., 2011). A first explorative 815 m depth  
23 continuous core (Pte-1 borehole) was drilled by Energia Andina on the  
24 southwestern flank of the volcanic complex (Fig. 1). The well lithology, dominated  
25 by Pliocene basaltic andesite lava flows and minor intercalated volcanoclastic  
26 layers, is summarized in Fig. 2. According to geological, geochemical and  
27 geophysical data, the geothermal reservoir could be hosted in the Oligo-Miocene  
28 volcanic and volcanoclastic units (not drilled in Pte-1 borehole) as well as in the  
29 lower part of the Pliocene volcanic sequences (Clavero et al., 2011).

30

1 Droguet et al. (2012) determined the geothermal alteration mineralogy of the  
2 Tinguiririca geothermal field (Fig. 2), using petrographic techniques, XRD and  
3 SEM. Samples were collected along the Pte-1 borehole, where the temperature  
4 was directly measured along the 813 m drill core. In the shallowest parts of the  
5 borehole (0-410 m), varieties of silica (mostly chalcedony according to  
6 petrographic characteristics) and iddingsite are present as index phases and  
7 hydrated Ca-Al silicates like wairakite (XRD and optical identification), prehnite  
8 and epidote together with quartz appear in the deepest ones (600-813 m)  
9 developing propylitic alteration consistent with almost neutral pH fluid conditions.  
10 The alteration minerals appear filling open spaces (voids and fractures), in the  
11 volcanic groundmass and as pseudomorphous of primary (mostly plagioclase)  
12 phases (Fig. 3).

13

### 14 **3. Material and methods**

15 Eighteen samples were selected along the Tinguiririca borehole for clay mineral  
16 characterisation using X-ray diffraction (XRD) and, from them, four samples were  
17 chosen for high-resolution and analytical transmission electron microscopy  
18 (HRTEM-AEM).

19 The depths of the samples studied along the borehole are shown in Fig. 2. The  
20 rocks of the drill core show a compact texture and small grain size, showing  
21 intense clay alteration inside the vitreous matrix. The color of the samples along  
22 the borehole is generally dark grey, with greenish tones at some depth of the  
23 upper part of the borehole. The vein fillings of calcite and various silica phases  
24 are common along the borehole.

25

26 Fig. 2 shows the alteration mineralogy determined by Droguet et al (2012) along  
27 the hole and the directly measured temperature during drilling. In the following,  
28 the samples will be named according to their depth in meters.

29

30 The samples were crushed with a laboratory jaw-crusher. The <2  $\mu\text{m}$  fraction  
31 was separated by centrifuge, and then smeared onto glass slides. In some



1 cases, it was necessary to remove the carbonates. A solution of 0.2 N HCl was  
2 added to the suspension of crushed rocks and agitated continuously for 10 min.  
3 We have used the recommendations by Moore and Reynolds (1997) in order to  
4 identify the different kind and proportion of the mixed layer minerals.

5  
6 The XRD data were obtained with three different diffractometers (1) Philips PW  
7 12050/25 powder diffractometer with  $\text{CuK}\alpha$  radiation at Mineralogic & Petrologic  
8 Solutions Ltd (New Zealand); (2) Philips PW 1710 powder diffractometer with  
9  $\text{CuK}\alpha$  radiation, graphite monochromator and automatic divergence slit at the  
10 Department of Mineralogy and Petrology of the Universidad de Granada and (3)  
11 Bruker D8 Advanced diffractometer with  $\text{Cu-K}\alpha$  radiation with a Bragg-Brentano  
12 geometry at the Department of Physics in the Faculty of Sciences and  
13 Engineering of the Universidad de Chile. Clay minerals in this fraction were  
14 identified according to the position of the basal reflections on XRD patterns of air-  
15 dried, ethylene-glycolated (EGC), and heated (300°C for 2 h). Illite-smectite (I-S)  
16 and Chlorite-smectite (C-S) mixed-layer clay minerals were identified and the  
17 respective proportions of illite and chlorite components determined according to  
18 Moore and Reynolds (1997) criteria. Heat treatments were useful for the  
19 identification of vermiculite layers in the chlorite mixed layered phases.

20  
21 The HRTEM studies were performed using two high resolution microscopes at  
22 the Universidad de Granada (Spain): (1) a Philips CM-20 scanning transmission  
23 electron microscope (STEM), working at 200 kV with a point to point resolution of  
24 2.7 Å in the TEM mode. 2) A Titan with XFEG emission gun, spherical aberration  
25 corrector and HAADF detector, working at 300 kV, with a resolution of 0.8 Å in  
26 the TEM mode and 2 Å in the STEM mode. Copper rings were attached to  
27 representative selected areas of the matrix of the thin-sections. These areas  
28 were detached through gentle heating. Samples were further thinned with a  
29 Gatan dual ion mill using an acceleration voltage of 6 kV during three stages: (1)  
30 incidence angle of 15° and probe current of 1 nA; (2) incidence angle of 15° and  
31 probe current of 0.6 nA; (3) incidence angle of 12° and probe current of 0.4 nA.

1 Chemical analyses of clay minerals were made in STEM mode with an EDAX  
2 microanalysis system. A  $200 \times 1000 \text{ \AA}$  scanning area with the long axis oriented  
3 parallel to phyllosilicate packets was used for each analysis using a  $50 \text{ \AA}$  beam  
4 diameter. Chemical compositions were obtained from two kinds of samples: from  
5 the copper rings, previously described, to correlate chemical compositions with  
6 high resolution images and from individual particles from powdered portions,  
7 dispersed onto C-coated Cu grids. The data thus obtained are complementary to  
8 those taken from ion-milled samples as their orientation allows the use of a larger  
9 scanning window for analysis, which provides better reproducibility of data and  
10 less loss of alkalis. Counting times of 100 s were used except for Na and K,  
11 which were analyzed using 30 s counting times (Nieto et al., 1996). Albite,  
12 olivine, biotite, spessartine, muscovite, chlorite and titanite were used to obtain K  
13 factors for transformation, according to Cliff and Lorimer (1975).

14

## 15 **4. Results**

### 16 *4.1. X-ray diffraction*

17 The mineralogy of the clay fraction determined by XRD and corresponding  
18 treatments is showed in Fig.2. Mixed layers, such as Illite-Smectite (I-S),  
19 corrensite (Corr) and Chlorite-Vermiculite (C-V) have been identified in several  
20 segments of the borehole from Tinguiririca geothermal fields.

21

22 I-S mixed layers has been determined comparing the air-dried and ethylene  
23 glycol treated specimens (Fig. 4a). Illite proportion of I-S was determined by the  
24 position of the reflection near  $16$  to  $17^\circ 2\theta$  and the ordering type by the position of  
25 the reflection from  $5$  to  $8.5^\circ 2\theta$  for ethylene glycol solvated preparations (Fig. 4a).

26

27 Chloritic-like phases with a more intense  $14 \text{ \AA}$  peak than the  $7 \text{ \AA}$  one have been  
28 observed in air-dried samples from several segments of the borehole (e.g. Fig.  
29 4b). We have compared the air-dried and  $300^\circ \text{ C}$  heated samples for determining  
30 the kinds of phyllosilicate layers present. Fig. 4 shows peaks on the sloping  
31 background at  $\sim 28 \text{ \AA}$  in the air-dried sample, which is also compatible with the

1 presence of corrensite. Low-charge corrensite appears in some samples,  
2 detected by the 28 Å peak which expands to 31 Å after EG-solvation (Fig. 4a and  
3 b). Heat treatment at 300 °C for 2 h resulted in one plateau with spacings ranging  
4 from 7 to 8 Å, respectively (Fig. 4b). This broad plateau is interpreted as a  
5 convolution of 002 (~7 Å) of chlorite and 003 (~ 8 Å) of collapsed corrensite.  
6 High-charge corrensite has been detected by the presence of the peak at 28 Å,  
7 which is unaffected by EG-solvation. Heat treatments also reveal the presence of  
8 a chlorite-vermiculite mixed layer in some samples. The presence of vermiculite  
9 layers generates significant changes in the intensity and basal spacing of  
10 chlorite. In this way, 001 of chlorite is 14.22 Å in air-dried samples, while in the  
11 heated samples appear the characteristic peak of chlorite at 14.13 Å. Both kinds  
12 of corrensite coexist in some samples (e.g. Fig. 4a). The peak deconvolution at ~  
13 29 Å in EG samples (not shown), confirms the presence of two peaks, one at 31  
14 Å and the other at 28 Å, corresponding respectively to low and high charge  
15 corrensite.

16

17 The distribution of the clay minerals along the borehole shows a zonation  
18 according to the depth (Fig 2). Smectite is present at the shallow parts of the  
19 borehole together with berthierine, identified by their peaks (001) at 7.07Å and  
20 (002) at 3.54Å. Below, I-S mixed layers appear instead of smectite. Interstratified  
21 clays show progressive illitization with increasing depth, from 60% of Illite layers  
22 with R1 order at 325 m to more than 90% of Illite layers with R3 order from 408  
23 m. From this depth, I-S R3 mixed layers with minor content of expandable layers  
24 (<10% of smectite) have been identified. Chlorite and high-charge corrensite  
25 appears together with I-S mixed layers. C-V mixed layers only were identified at  
26 408m. Low-charge corrensite was identified at the bottom of the borehole. At this  
27 depth chlorite is present in addition to low-charge corrensite.

28

#### 29 *4.2. Transmission electron microscopy*

30 Selected samples representing each of the phyllosilicate mineral zones found by  
31 XRD (Fig. 2) were examined by TEM in order to characterize the mineralogy,

1 textural relationships and chemical composition of the clay minerals along the  
2 borehole.

3  
4 Typical TEM textures from each depth are shown in Fig. 5. At low magnification,  
5 TEM images show similar textures in the analyzed samples. Clay minerals  
6 replace plagioclase and volcanic glass and show curved, lens-shaped  
7 morphology and no preferred orientation. Smectite appears filling pores inside of  
8 plagioclase crystals at 158m of depth (Fig. 5a). Smectite shows a ribbon-like  
9 morphology (Güven and Grim, 1972; Grim and Güven, 1978). I-S mixed layers  
10 can be recognized at the HAADF image of sample 328 showing a similar texture  
11 to smectite (Fig. 5b), with curved and lens-shaped morphology and no preferred  
12 orientation. Volcanic glass has been recognized in sample 328 by its composition  
13 and completely amorphous character (absence of diffraction spots in SAED). It is  
14 apparent from Fig. 5c the genetic relationship between glass and the process of  
15 dissolution-precipitation which occurred during the crystallization of I-S mixed  
16 layers. Low-charge corrensite appears filling irregular cavities of plagioclase,  
17 providing direct evidence for neocrystallization from hydrothermal fluids (Fig. 5d).

#### 18 19 *4.2.1. Sample 158*

20 Smectite packets exhibit a lens-shaped morphology in TEM images, with no  
21 preferred orientation (Fig. 6a). The smectite is characterized by discontinuous,  
22 wavy fringes, with d-spacings of 10 Å. The smectite layers are curved with their  
23 orientation changing along the packet and the number of parallel layers is very  
24 small, frequently lower than four. The various sub-packets, considering these as  
25 areas constituting a coherent crystalline domain, show an anastomosing  
26 relationship to each other, with frequent layer terminations at low-angle contacts  
27 with the neighbour sub-packet. In Fig. 6b, partial two-dimensional resolution  
28 allows measuring 4.5 Å as the crystalline parameter along the layers. This  
29 distance corresponds to half b parameter of the phyllosilicates (reflection 020). In  
30 those areas in which the two-dimensional resolution persists at less for three  
31 lattice fringes, local coherence between the parallel layers may be recognized,

1 with the fringes perpendicular to the smectite layers and showing continuity from  
2 layer to layer. In adjacent layers also an angle of  $\sim 60^\circ$  may be measured  
3 between the two families of fringes, which, according to Dong and Peacor (1996)  
4 correspond to the (112) reflection. This situation is similar to the case described  
5 by Dong and Peacor (1996) for Gulf Coast smectites and coherent with the  
6 model proposed by Guthrie and Reynolds (1998).

7  
8 Minor packets showing  $7\text{\AA}$  spacing are visible in some areas. Peaks  
9 corresponding to such spacing are absent in the XRD diagram, probably due to  
10 their rarity in the sample; however berthierine was identified by XRD in sample  
11 262. Therefore, we tentatively interpret those fringes as corresponding to  
12 berthierine.

#### 13 14 *4.2.2. Sample 328*

15 Fig. 7 shows typical lattice fringe images of this sample. Illite-smectite mixed  
16 layers show defective texture similar to smectite from sample 158. In this way,  
17 the I-S displays curved small packets (25 nm thick), similar to the smectite (Fig.  
18 7a). Also an anastomosing relationship between the various sub-packets is  
19 evident. Consequently in most of the cases the crystalline domain size is formed  
20 by no more than 4-10 layers.

21  
22 In some areas, fringes show alternating dark and light contrast, typical of I-S  
23 mixed-layers (Fig. 7b). Guthrie and Veblen, (1989a and b, 1990) and Veblen et  
24 al. (1990) described that in normal routine conditions smectitic and illitic layers  
25 cannot be distinguished, but some particular conditions in the TEM can allow  
26 their differentiation. Therefore, we can expect packets formed by  $10\text{\AA}$  layers as  
27 those shown in Figure 7a. Differences of contrast will be visible only in some  
28 particular areas (Fig. 7b), which fulfil the particular conditions necessary to  
29 produce differences of contrast or spacing. Fringes with spacing of 22, 32 or  $35\text{\AA}$   
30 periodicity, characteristic of the sum of one or two illite and one smectite layer  
31 spacing in R=1 I-S (Kim et al., 1995; Dong et al., 1997) can also be recognized.

1 Non-001 reflections are ill-defined, nonperiodic and diffuse parallel to  $c^*$  (Fig. 7a,  
2 inset), implying that stacking is generally random. Such SAED patterns have  
3 commonly been found to be diagnostic of  $1M_d$  polytypism.

4  
5 Chlorite is usually intergrown and/or interstratified with 10 Å and 7Å layers (Fig.  
6 7c and d). In some cases small packets (20 nm thick) of pure chlorite may be  
7 recognized. The presence of 10 Å layers is coherent with the XRD results, which  
8 have shown chlorite and corrensite in the samples of this part of the borehole.  
9 Intermixing and interlayering of berthierine have been frequently described in  
10 low-temperature chlorite and it is a consequence of the metastable character of  
11 the former (Abad and Nieto, 1995 and references therein). SAED always shows a  
12 disordered polytype for chlorite (Fig. 7c and d, inset), which, at least in part, may  
13 be a consequence of the previously described interstratified layers.

#### 14 15 *4.2.3. Sample 653*

16 Small packets of illite have been observed in sample 653, with a typical packet  
17 size of 30 nm thick (Fig. 8a and b). Curvature and the general high defective  
18 character of previously described samples are absent (Fig. 8a and b). Straight  
19 boundaries and defect-free lattice fringes are a renowned characteristic. The size  
20 and characteristics are similar to those typical of the low-anchizone in diagenetic  
21 evolution (Merriman and Peacor, 1999). High magnification images show the  
22 presence of lattice fringes with spacing of 10 and 20 Å. Differences in contrast or  
23 spacing, indicative of minor smectite layer presence have not been recognized.  
24 Nevertheless, as stated by Guthrie and Veblen (1989a), this fact is not conclusive  
25 about the complete absence of smectite layers and, according to the XRD, illite-  
26 smectite (I-S) mixed-layers with R3 order and a content of illite layers higher than  
27 90% are the dominant illitic phase. We assume, therefore, that minor smectite  
28 layers should be present but they are not distinguishable from the illitic layers.

29  
30 Two kinds of SAED patterns for the illite packets have been recognised: (1)  
31 SAED patterns with well defined (00l) reflections at 10 Å, with diffuseness normal

1 and parallel to  $c^*$ , implying that stacking is generally random and therefore  
2 corresponding to  $1M_d$  polytypism (Fig. 8a); and (2) SAED patterns with non -001  
3 reflections showing a well defined periodicity at  $20\text{\AA}$ , indicating that they  
4 correspond to a well-ordered 2-layer polytype (Fig. 8b), probably  $2M_1$ . The 001  
5 row has additional weak reflections producing  $20\text{\AA}$  periodicity due to dynamical  
6 effects. No relationship between size of packets and polytype has been found.

7  
8 Usually, at least two different orientations are recognized in the SAED. One  
9 includes  $c^*$  and  $b^*$  (or equivalent direction) and the other  $c^*$  and  $a^*$  (or equivalent  
10 direction). Normally a SAED is obtained from an area that includes various  
11 packets. These packets are differently oriented in relation to the  $c^*$  direction, but  
12 also in the  $a^*-b^*$  plane.

13  
14 Chlorite (Fig. 8c) is present in small packets (20 nm). They are often free of  $10\text{\AA}$   
15 layers. Their polytype always appears disordered (Fig. 8c inset).

#### 16 17 *4.2.4. Sample 776*

18 The major phyllosilicate in the sample is chlorite, which presents variable  
19 interstratification with  $10\text{\AA}$  layers (Fig. 9). In some cases packets showing  $24\text{\AA}$   
20 layers can be recognized (Fig. 9a). They represent the ordered sum of one  
21 chlorite layer ( $14\text{\AA}$ ) and one contracted smectite layer ( $10\text{\AA}$ ). Overall, the sample  
22 is composed of chlorite and low-charge corrensite, which can be partially,  
23 interstratified with each other, giving major  $14\text{\AA}$  spacing with less  $10\text{\AA}$  layers (Fig.  
24 9b). Similar textures were described by Kogure et al. (2013), for their samples,  
25 where generally the corrensite-chlorite layers were often curved in their cross-  
26 sectional views. Lenticular voids are common in the crystals, which were  
27 presumably formed by the collapse of hydrated smectite-like interlayers in the  
28 vacuum environment during ion-milling and/or TEM examination. Illite is also  
29 present as a minor phase in the sample, as also indicated by the presence of a  
30 weak peak at  $10\text{\AA}$  in XRD diagrams. Lattice fringes of  $20\text{\AA}$  have been  
31 recognised in some images, which indicates illite with 2M polytype.

1

## 2 *4.3. Analytical electron microscopy*

### 3 *4.3.1. Smectite and illite-smectite mixed-layers.*

4 Table 1 presents the analyses corresponding to smectite and intermediate illite-  
5 smectite compositions. They correspond in all cases to dioctahedral  
6 compositions. In some cases, the octahedral sum is slightly higher than normal.  
7 Two causes for this are possible; one is that Na could not be determined on  
8 copper grid preparations due to the overlapping of the L line of copper, but  
9 according to ion milling sample analyses, is present in minor proportions. This  
10 deficit of positive charge produces an artificial slight increase of the overall  
11 number of cations. The second cause is that a part of Mg, which, in the absence  
12 of a valid criterion of distribution, we have totally assigned to the octahedral  
13 position, may be also in the interlayer.

14

15 Smectite in sample 158 presents more homogeneous compositions than I-S in  
16 samples 328 and 653, which considerably overlap their respective fields of  
17 composition (Fig. 10). Smectites have the highest Fe and Mg contents, reflecting  
18 their montmorillonite-nontronite composition and very limited beidellitic  
19 component. The sum of these two elements is similar in samples 328 and 653,  
20 but the latter present lower values for some particular analyses (Fig. 10). The  
21 ratio between the two elements is different from sample 328 to 653. The major  
22 interlayer cation in smectite is Ca.

23

24 Samples 328 and 653 have a lower Si content and higher interlayer sums (Fig.  
25 10) in comparison to smectites of sample 158, differences which are coherent  
26 with their more illitic composition. Plotted in the Velde (1985) diagram, the three  
27 samples show evolution toward a more beidellitic and/or illitic character with  
28 increasing depth (Fig. 11). In fact, some of the analyses in sample 653 clearly  
29 reach the field of muscovite compositions (Table 1). Nevertheless, the  
30 corresponding compositional fields are far to be clearly separated; significant  
31 overlap of the fields corresponding to the three samples exists.



1

2 Sample 653, characterized by R3 I-S shows the highest K and interlayer cations  
3 content and the lowest Si content. Sample 328, containing R1 I-S mixed layer  
4 phases, presents an intermediate composition between 158 and 653 (Fig. 10).

5

6 The increase of negative tetrahedral charge, linked to Si diminution from more  
7 smectitic compositions toward the more illitic ones is basically compensated for  
8 by interlayer charge increase. Nevertheless, an additional mechanism for  
9 compensation linked to Mg substitution by trivalent cations is also observed on  
10 Fig. 10. Therefore, together with the classical  $\text{Si}^{4+} + \square \rightarrow \text{Al}^{3+} + \text{K}^+$  we find also a  
11  $\text{Si}^{4+} + \text{Mg}^{2+} \rightarrow \text{Al}^{3+} + \text{Al}^{3+}$  compositional vector, that is, a decrease of tschermack  
12 component, which brings the I-S toward more muscovitic compositions. This  
13 chemical evolution can be also observed on the Velde (1985) diagram (Fig. 11)  
14 by the progressive displacement of the compositions toward the 3R2+ free side  
15 of the triangle. In addition to these two chemical changes, also a decrease in Fe  
16 content may be observed from the smectitic to the illitic samples.

17

#### 18 *4.3.2. Chlorite and corrensite*

19 The majority of analyses obtained on major 14Å areas show mixed  
20 characteristics between those of pure chlorite and pure corrensite (Fig 12).  
21 Nevertheless, some extreme analyses produce formulae, which can be  
22 considered as pure chlorite (Table 2) and corrensite respectively (Table 3). The  
23 rest of the compositions can be considered as corresponding to chlorite-  
24 corrensite mixed layers, that is, compositions with a number of 14Å layers  
25 intermediate between 50% and 100%. In such cases the right number of oxygen  
26 atoms to be considered in the formula calculation would depend on the exact  
27 proportion of chloritic and smectitic/vermiculitic layers, hence it is different and  
28 unknown for each analysis, which precludes the conversion of such compositions  
29 in mineral formulae.

30

1 Corrensite composition (Table 3 and Fig. 12) is highly heterogeneous at the level  
2 of the sample, and from sample to sample. Overall octahedral sums approach 9,  
3 therefore, presumably, it is trioctahedral, for the two components; however they  
4 show some minor variable deficits, which is higher for sample 328 than for 776.  
5 The Fe and Mg contents are similar each other and high, with no significant  
6 differences between the samples. Sample 776 presents clearly lower Al content  
7 and generally higher Si content than 328. The interlayer sum is similar between  
8 the two samples, but the major interlayer cation is K for sample 328, while Ca is  
9 clearly predominant in 776.

10  
11 Chlorite also displays a very heterogeneous composition (Table 2 and Figs. 12  
12 and 13). The majority of the analyses show high Si content and low octahedral  
13 sums, both typical characteristics of low temperature chlorites (Vidal et al., 2005,  
14 Inoue et al, 2009). Nevertheless, some significant exceptions may be found, with  
15 the two chemical parameters clearly different from the general tendency of the  
16 sample (Fig. 13 and Table 2). No clear relationship exists between such  
17 differences and a possible contamination by dioctahedral phases, evaluated  
18 through the interlayer cation content of each individual analysis (Table 2). In  
19 general Mg content is slightly higher than Fe, with no clear differences among the  
20 three samples.

21  
22 In the R<sub>2</sub>+Si diagram of Wiewióra and Weiss (1990) most of the chlorite  
23 compositions concentrate between the clinocllore, sudoite and corundophullite,  
24 though some extension was observed toward Al-free chlorite (Fig. 13). However,  
25 corrensites show clearly different compositions, significantly closer to sudoite.

## 26 27 **5. Discussion**

### 28 *5.1. The vertical distribution of clay minerals*

29 Different clay mineral assemblages have been recognised along the Pte-1 drill  
30 hole from the Tinguiririca geothermal field in the Andean Cordillera of central  
31 Chile, which have allowed us to organize them in four main clay mineral

1 alteration zones: (1) alteration zone I (from 0 to 300 m) dominated by smectite,  
2 (2) alteration zone II (from 300 to 410 m) dominated by R1 I-S mixed layers,  
3 chlorite and high-charge corrensite ; (3) alteration zone III (from 410 to 700 m)  
4 dominated by R3 I-S mixed layers, chlorite and high-charge corrensite; (4)  
5 alteration zone IV dominated by low-charge corrensite and chlorite.

6

7 The smectite to illite sequence is discontinuous, according to XRD. A smectite-  
8 rich I-S zone between zone 1 (smectite) and zone 2 (R1) has not been identified.  
9 TEM data also agree with XRD. We have not identified R0 I-S, whose major  
10 component was smectite. Therefore, apparently the change from alteration zones  
11 I to II is discontinuous. Nevertheless, a more exhaustive sampling of this part of  
12 the sequence would be useful to clarify this point.

13

#### 14 *5.1.1. Smectite and I-S mixed layer zones: I-S formation*

15 The shallow zone is characterised by the presence of aluminous clay phases  
16 (smectite, scarce berthierine, and I-S mixed layers) associated with pyrite, and  
17 hematite. The clay mineral assemblages developed at 158 m consist mostly of  
18 smectite. The chemical composition of the smectite is coherent with a  
19 montmorillonite with high nontronitic component and very low beidellitic  
20 component. Such composition is typical of smectites related with a significant  
21 volcanic input, such as an early alteration product of volcanic glass (eg. Bauluz et  
22 al. 2000, 2002; Guisseau et al.; 2007).

23

24 Regularly ordered I-S mixed layers have been identified from 325 m to 661 m.  
25 The content in expandable layers of this I-S mixed layers decrease with the depth  
26 and temperature, indicating a prograde reaction of smectite to illite via I-S mixed  
27 layers, in the presence of near neutral geothermal waters (Reyes, 1990). The  
28 reaction of smectite to illite, via I-S mixed layers has been widely reported in  
29 hydrothermal and diagenetic systems. Previous studies of I-S minerals  
30 suggested an illitization sequence, which was apparently continuous from  
31 smectite through I-S phases to illite (eg. Harvey and Browne, 1991). This

1 transition of smectite to illite has been considered as the result of a thermally  
2 active sequential transformation reaction from smectite precursor to illite which  
3 proceeds via crystallization of I-S mixed layers series (Meunier and Velde, 1989)  
4 or as a result of simultaneous crystallization of all the I-S mixed layers via direct  
5 precipitation from solution (Inoue et al., 2004). In the Tinguiririca geothermal  
6 fields, the variation in the proportions of smectite (S) and illite (I) layers in the I-S  
7 minerals can be correlated directly with the temperature.

8  
9 The textural evidences of clay minerals under TEM and in addition to the thin-  
10 section observations, indicates that primary minerals were in part dissolved by  
11 hydrolytic reaction and the smectite and I-S mixed layers precipitated *in situ* from  
12 the altering solutions. The typical defective characteristics of smectite, with layer  
13 terminations, dislocations, contrast changes, are also observed in the I-S mixed  
14 layers (Figs. 5 and 7a and b) indicating that these phases are involved in the  
15 prograde reaction. This reaction was detected from 325 to 408 m, where ash-  
16 dominated volcanic rocks are cut by the borehole. It is known that solutions  
17 reacting with vitric materials at a given temperature might increase in pH and  
18 dissolved solids, enriching the solution in Mg, Ca and Na as well as SiO<sub>2</sub>. The  
19 resulting high pH and Na solution favours the formation of smectite (eg. Hay and  
20 Sheppard, 2001; Inoue et al., 2004). Due to a higher temperature in the 325 –408  
21 m intervals, the hydrolytic reaction forms aluminous I-S minerals instead of  
22 montmorillonite by incorporating K ions into the structure from ambient solutions.

#### 23 24 5.1.2. R3 I-S zone:

25 The following zone is characterised by the presence of illite rich I-S, corrensite  
26 and chlorite as the main phyllosilicates and Ca-silicates (wairakite, prehnite,  
27 epidote and titanite). The illite in this zone corresponds to an illitic phase with low  
28 expandable component (<10% of smectite). The HRTEM data show that the  
29 sample at 653 m is composed of intergrowths of illite and chlorite. At this depth,  
30 the illite has straight boundaries and defect-free lattice fringes indicating a lower  
31 defective character than those formed in the shallower parts. The illite polytype

1 observed are 1M<sub>d</sub> and 2M. Therefore, at this depth the illite features are typical of  
2 higher temperatures. The existence of differences of composition between the  
3 areas which show SAED typical of 1M<sub>d</sub> and 2M polytypes could indicate the  
4 beginning of the transition from the R3 I-S zone to the illite *sensu stricto* zone, with  
5 coexistence of the two kinds of illitic materials, showing differences in polytype  
6 and composition. In fact, some typical analyses corresponding to mature micas  
7 may be found in Table 2 (e. g. 653-2, 653-1A and 653-2A). The coexistence of  
8 various types of I-S materials at the sample level is a proven fact, frequently  
9 described in the literature (e.g. Nieto et al., 1996, Ferrage et al., 2011).

### 11 5.1.3. *Corrensite and chlorite: corrensite formation*

12 The mineral assemblages of altered rocks below 735 m until the bottom of the  
13 borehole reveal the presence of low-charge corrensite and chlorite. The transition  
14 of smectite to chlorite consists of the formation of chlorite-smectite (C-S)  
15 irregularly mixed layered (e.g. Bettison et al., 1991; Schiffman and Fridleifsson,  
16 1991; Robinson and Bevins, 1994; Meunier et al., 2008a; Meunier et al., 2008b;  
17 Leoni et al., 2010) or by discontinuous changes from smectite to corrensite to  
18 chlorite without irregularly mixed-layered chlorite-smectite (e.g. Inoue et al., 1984;  
19 Shau et al., 1990; Inoue and Utada, 1991; Schiffman and Staudigel, 1995;  
20 Schmidt and Robinson, 1997; Beaufort et al., 1997). The increase in chlorite  
21 content often is related with an increase in temperature (Schiffman and  
22 Fridleifsson, 1991). Corrensite occurs between 100 and 200°C (Inoue and Utada,  
23 1991). The complete change of corrensite to discrete chlorite is completed above  
24 240° C (eg. Kristmannsdóttir, 1976; McDowell and Elders, 1980, 1983; Keith and  
25 Bargar, 1988). High chlorite content can also be related to high fluid/rock ratio or  
26 mineral alterations, which provide the Al needed to form chlorite (Shau and  
27 Peacor, 1992; Schmidt and Robinson, 1997).

28  
29 Low-charge corrensite and discrete chlorite in our samples appear at  
30 temperatures measured in the borehole of 220°C. This temperature is too high  
31 for the stability field of corrensite. However, the application of the Bourdelle

1 geothermometer in chlorites from sample 776 indicates a temperature of  
2 formation for one group of chlorites around 140°C, which is perfectly coherent  
3 with the presence of low-charge corrensite and chlorite in sample 776. Therefore,  
4 in the Tinguiririca samples the presence of corrensite at the bottom of the  
5 borehole shows that the alteration temperature was lower than the present-day  
6 temperature.

7

## 8 *5.2. Chemical evolution of I-S*

9 The knowledge of the chemistry of I-S phases and the limits of their  
10 compositional fields has been hindered by their defective character, small size  
11 and lack of adequate analytical methods. Consequently, their compositional fields  
12 are still obscure and a lack of a definition of typical chemical compositions still  
13 exists in the mineralogical literature, which does not allow their unambiguous  
14 identification based only on their chemical composition.

15

16 The presented results for the Tinguiririca borehole Pte-1 offer an opportunity to  
17 extend the knowledge of the chemical compositions and evolution with  
18 temperature and depth of their chemistry. The mineralogy is relatively simple,  
19 with virtual absence of detrital phases and the calculated formulae are based on  
20 high quality analyses. We have combined two kinds of preparations of samples to  
21 have the opportunity of referring the obtained compositions to given textural  
22 positions and high-resolution images and, at the same time, using the best  
23 possible analytical conditions in AEM (see Methods section). The two kinds of  
24 analyses have defined the same compositional fields for each of the studied  
25 samples with no significant differences in relation to the two kinds of preparations  
26 (compare in Table 1 the formulae labelled with A, after the number, obtained on  
27 ion-milled samples with those without A, obtained on grid samples). A former  
28 version of Figs. 10 and 11, differentiating the two kinds of analyses (not shown,  
29 for simplicity) showed no-difference between them. Therefore we are confident  
30 that the overall set of analyses represent the corresponding phases shown in the

1 high-resolution images and, at the same time, offer the maximum analytical  
2 quality that the currently available methods can offer.

3  
4 Given the respective chemical composition of smectite and illite and the partial  
5 former results about the I-S chemistry, it has been assumed that more mature I-S  
6 should be characterized by a diminution of the pyrophyllitic component toward a  
7 theoretical muscovite. In other words, we could expect for illite-richer I-S higher  
8 interlayer charge, particularly related with K increase, which balances a  
9 diminution of the tetrahedral charge due to the increase of Al and decrease of Si.  
10 The Tinguiririca results, shown in Fig. 10, perfectly confirm this broad tendency  
11 and can be considered as conclusive for such a prediction.

12  
13 Nevertheless, when the results presented on Fig. 10 are considered in detail, we  
14 can establish two refinements to this general conclusion. The first one is the  
15 existence of a second chemical balance which compensates the Si decrease in  
16 addition to the diminution of the pyrophyllitic component, based on a coeval  
17 decrease of the tchermack component, that is, a substitution of Mg+Fe by Al in  
18 the octahedral layer. The second one is the highly heterogeneous character of  
19 the compositional fields of the implied phases. The respective fields of  
20 compositions broadly overlap each other, making a definition of differentiated  
21 fields for each of the types of I-S mixed layers impossible. In other words, I-S  
22 mixed-layer types cannot be distinguished based only on chemical compositions.

### 23 24 *5.3. Relationship between measured temperature and I-S mineral changes*

25 Many authors have focused their studies on establishing the temperatures of the  
26 transformations in the system smectite-I-S-illite. Generally, the temperatures  
27 where I-S mixed layers R1 with approximately 50-60 % of illite layers appears in  
28 diagenetic environments are in the range from 75 to 120° C (Hoffman and Hower,  
29 1979; Srdonon and Eberl, 1984; Schegg and Leu, 1996; Usysal et al., 2000; Adid  
30 et al., 2004). Libbey et al. (2013) also showed a positive correlation between the  
31 proportion of illite in the I-S interlayer and downhole temperature in the Te Mihi

1 area, Wairakei geothermal field (New Zealand), even suggesting a local I-S  
2 geothermometer based on the illite proportion. In the Tinguiririca borehole the  
3 last smectite sample corresponds to a temperature of 80°C and the first one in  
4 which this last has been replaced by R1 I-S to 120°C. Therefore, a temperature  
5 around 100°C, perfectly compatible with the previous range defined in the  
6 literature, may be considered as a valid reference for this first step of the  
7 transformation from smectite to illite.

8  
9 The transition from R1 to I-S R3 with more than 85 % of illite layers has been  
10 described in the diagenetic literature at 150-190° C (Hoffman and Hower 1979;  
11 Weaver 1989; Lindgreen 1991; Pollastro 1993; Abid et al., 2004). In our case, I-S  
12 mixed layers appear with R3 ordering and 90% of illite layers at 408m. The  
13 measured temperature in the borehole was of 125°C at 325 m, suddenly  
14 increasing to 180°C at 408 m. Therefore the temperature of the sequence of  
15 increasing illite and ordering of I-S mixed layers agrees well with the temperature  
16 previously exposed.

17  
18 Previous comparisons are based on the extensive literature about diagenetic  
19 environments. The extent at which they can be extended to a hydrothermal  
20 environment is unknown. Some papers have emphasized the fact that the  
21 different steps of the transformation process can be retarded in terms of  
22 temperature by scarce disposability of reactants due to lack of porosity and low K  
23 content. For example, Arostegui et al. (2006) found temperatures of 160°C for the  
24 disappearance of smectite and 240°C for the R1-R3 transition in marly  
25 lithologies. As an opposite case, the open crystallization from a fluid rich in the  
26 illite components in a geothermal field offers an ideal environment for the  
27 transformation. Other geological environments, as with the diagenetic one, could  
28 increase such temperatures due to local factors.

29  
30 Finally, it is highlighted that the transformation into pure illite has not been  
31 completed at the bottom of the borehole, with some minor residual smectitic



1 layers even at temperatures as high as 220°C. The difficulty of the completeness  
2 of the reaction based only on thermal effects, without tectonically induced strain  
3 as a driving force for the reaction, is a widely accepted fact in the incipient  
4 metamorphism literature (Merriman and Peacor, 1999).

#### 5 6 *5.4. Chlorite thermometry*

7 Discrete chlorite displays a wide range of non-stoichiometric compositional  
8 variations depending on bulk rock composition and physicochemical conditions  
9 prevalent at the formation. The variation of chemical composition in chlorite  
10 therefore is useful to obtain information on the physicochemical conditions of the  
11 formation, such as the temperature. However, chlorite geothermometry has been  
12 a widely controversial matter during years (Cathelineau, 1988, de Caritat et al.,  
13 1993, Lopez-Munguira et al., 2002, Vidal et al., 2005, 2006, Inoue et al, 2009).  
14 The first geothermometers proposed by Cathelineau and Nieva (1985) and  
15 Cathelineau (1988) were based on direct empirical relationships between some  
16 chemical parameters and measured temperatures in geothermal areas (Los  
17 Azufres, Mexico), but it was questioned that they were widely affected by small  
18 scale interstratifications and intergrowths and are not based on chemical  
19 equilibrium (Essene and Peacor, 1995). Therefore, the empirical relationship was  
20 only valid for the studied geological context. The introduction of Vidal and Inoue's  
21 thermodynamic geothermometers based on the overall composition of chlorite  
22 was a significant step. Nevertheless, their wide use was severely limited by the  
23 necessity of the  $Fe^{2+}/Fe^{3+}$  ratio of the chlorite, which is difficult for low  
24 temperature materials. Recently, Bourdelle et al. (2013) have published a new  
25 semi-empirical chlorite geothermometer, which does not require prior  $Fe^{3+}$   
26 knowledge, calibrated on 161 analyses with well-constrained T data covering a  
27 wide range of geological contexts and tested for low-T chlorites (T <350°C and  
28 pressures below 4 kbar).

29  
30 We have applied the Bourdelle geothermometer to Tinguiririca chlorite phases.  
31 According to the Bourdelle et al. (2013) recommendation, chlorite must be free of

1 10 Å layers. We have then limited the application of the geothermometer only to  
2 analyses producing formulae with less than 0.10 interlayer charge. Fig. 2  
3 compares the obtained temperatures with those directly measured in the  
4 borehole.

5

6 In broad outlines, some differences have been observed between the empirical  
7 temperatures calculated using chlorite chemical composition and the present day  
8 measured temperatures. The temperature obtained with the geothermometer in  
9 sample 328 is 178°C, which represents a difference with the temperature  
10 measured in the borehole of around 50°C, which is the error margin of the  
11 Bourdelle geothermometer. Two temperatures calculated for sample 653 (653-17  
12 and 653-18) are exactly the same as the average temperature of the borehole at  
13 this depth. The temperature calculated using the 653-9A analysis is only 46° C  
14 lower than the average temperature in the borehole, being the difference also  
15 under the predicted error limits of the method.

16

17 Finally, the highest differences were obtained in sample 776 (bottom of the drill  
18 core). In fact, in this sample we can recognize two well defined groups of  
19 temperatures, which are clearly different to the 233°C of the measured  
20 temperature of the borehole at this depth. One group has an average  
21 temperature of 139° C and the other 346 °C. These two groups of temperatures  
22 are the consequence of two groups of chlorites in the sample with very different  
23 morphology and compositions (Figs. 12 and 13). One of the groups shows the  
24 chemical characteristics invoked by all the thermometric approaches for low  
25 temperature chlorites, that is, high Si and low octahedral population, being  
26 coincident with the chemical character of the rest of samples of the borehole. The  
27 other group of compositions shows just the opposite characteristics and,  
28 therefore, would produce higher temperatures independently of the used  
29 thermometric model. Hence, if we accept the thermodynamic basis of the chlorite  
30 thermometry, we need to admit the existence of two groups of chlorites in the  
31 sample formed at clearly different temperatures. These two chlorite groups were

1 then formed during two different alteration events along the evolution of the  
2 Tinguiririca geothermal field. Moreover, the chlorites of lowest temperatures  
3 would be not in equilibrium with hydrated Ca-Al silicates (wairakite, epidote and  
4 prehnite) observed in the lower part of the core with the temperature of formation  
5 normally higher than the calculated by means of chlorite thermometry for this  
6 group of analyses. Wairakite is normally described in geothermal systems  
7 worldwide to be stable in the 200<sup>o</sup>-300<sup>o</sup>C interval, meanwhile epidote and  
8 prehnite are normally stable over 200<sup>o</sup>C (e.g. Browne, 1978; Henley and Ellis,  
9 1983; Reyes, 1990). Gas geochemistry geothermometry (H<sub>2</sub>-Ar, CO<sub>2</sub>-Ar and  
10 CO<sub>2</sub>-CH<sub>4</sub>) suggests equilibration temperatures in between 220<sup>o</sup> and >300<sup>o</sup>C for  
11 reservoir conditions (Clavero et al., 2011), in concordance with the highest  
12 temperatures obtained using chlorite thermometry and propylitic alteration  
13 mineralogy. Consequently, the low-T chlorite group could be in relation with the  
14 cooling of the system by cold water influx, as reflected by the present day  
15 measured temperature. Moreover, at these depths abundant hematite in veins is  
16 frequently observed (some of them centimetric in width) and clots in the matrix,  
17 interpreted by Reyes (1990) as indicative of cold water input into the geothermal  
18 system.

19 In any case, the persistence of two morphologically and chemically contrasted  
20 chlorite families indicates disequilibrium conditions and must be related with the  
21 kinetics of the alteration processes in geothermal systems. Contrary to diagenetic  
22 processes related to burial, geothermal alteration in active systems is related to  
23 rapid events that could preclude the achievement of equilibrium conditions.

24 Similar kinetic constraints were also previously proposed by Inoue et al (2004) to  
25 explain differences between present-day temperatures in geothermal systems  
26 and alteration mineral assemblages. Moreover, these authors remarked on the  
27 influence of the geologically short period of time during geothermal alteration and  
28 different fluids and processes involved in geothermal systems (boiling, mixing) in  
29 contrast to burial diagenesis. All these parameters are potentially misleading in  
30 terms of the relationship between the observed mineral assemblages and  
31 present-day temperature.

1 Consequently, we tentatively hypothesize that the temperatures around 346° C  
2 could be related with chlorites crystallised during the main alteration event  
3 affecting the Tinguiririca geothermal system. This high temperature event is  
4 consistent with the alteration mineralogy observed and estimations of reservoir  
5 temperature using gas and fluid geochemistry (Clavero et al., 2011). Continuous  
6 clay mineral evolution described from top to bottom of the studied core is also  
7 consistent with this increasing temperature with depth. On the contrary, the lower  
8 temperatures obtained, around 139° C, could indicate that these chlorites do not  
9 reflect the main hydrothermal event and could be related to a cold water influx  
10 locally affecting the geothermal system. More detailed studies concerning textural  
11 relationships between these two chlorites are necessary with the aim to identify  
12 the precise origin of them and define if low T chlorites developed over high-T  
13 ones or directly precipitated from hydrothermal fluids.

14

## 15 **6. Conclusions**

16 This study contributes to a better knowledge of the vertical distribution of the clay  
17 minerals assemblages close to 900 m below the surface area of the geothermal  
18 field of Tinguiririca in the Andean Cordillera of central Chile. The evolution with  
19 depth of clay mineralogy in this geothermal field is temperature-dependent and  
20 consistent with the classical pattern widely described in the hydrothermal and  
21 diagenetic literature. Moreover, the clay mineral evolution observed is also  
22 consistent, in general terms, with the present day temperature measured in the  
23 borehole. Clay minerals grew from solutions enriched in the necessary chemical  
24 components by the dissolution of pre-existing volcanic minerals and glass.  
25 Montmorillonitic smectite, at the top, evolved to R1 I-S at temperatures around  
26 100°C and these to R3 I-S at nearly 150°C. The concomitant chemical evolution  
27 implied two main compositional vectors toward an end-member muscovitic  
28 composition; the major one is the diminution of a pyrophyllitic component  
29 ( $\text{Si}^{4+} + \square \rightarrow \text{Al}^{3+} + \text{K}^+$ ), with some additional contribution of the reduction of the  
30 tschermack component ( $\text{Si}^{4+} + \text{Mg}^{2+} \rightarrow \text{Al}^{3+} + \text{Al}^{3+}$ ). Associated to the advent of R1  
31 I-S, Mg released by the latter reaction allowed the onset of chlorite, corrensite

1 and corresponding Chlorite-Vermiculite mixed-layers, which persist to the bottom  
2 of the borehole. The application of the semi-empirical chlorite geothermometer,  
3 newly developed by Bourdelle et al (2013) allows the determination of the  
4 alteration temperature conditions and contrasts with the present day temperature  
5 measured in the borehole. A general trend of increasing temperature with depth  
6 has been observed. However, in samples from the bottom of the drill hole, two  
7 populations of chlorite with diverse morphology, chemistry, calculated  
8 temperature and origins could be differentiated. The origin of these two chlorite  
9 families could be related to two different alteration events and the persistence of  
10 chlorites with different temperatures reflects disequilibrium conditions controlled  
11 by kinetic processes. The highest T chlorite could reflect the real thermal  
12 conditions during the main geothermal alteration and could indicate the minimum  
13 temperature of the reservoir conditions.

14

15 This investigation shows the importance of the study of clay minerals for  
16 geothermal exploration and evaluation of the future evolution of geothermal  
17 systems. Moreover, the combination of XRD and HR-TEM-AEM techniques gives  
18 fast and very reliable characterization of the different clay assemblages and allow  
19 the characterization of different clay minerals parageneses that could be related  
20 to different geothermal events. Only using high resolution techniques could make  
21 possible the identification of different clay mineral generations, allowing the  
22 development of alteration models for active geothermal systems.

23

#### 24 **Acknowledgements**

25 Authors thank Energia Andina company and, especially German Pineda and  
26 Richard Sutil, for the facilities in the access to the Pte-1 borehole samples. We  
27 also thank M.M. Abad (CIC, University of Granada) for her help with the HRTEM  
28 work. Financial support was provided by the Chilean Research Projects  
29 Fondecyt-Regular-1140629 and FONDAP-CONICYT-15090013 “Andean  
30 Geothermal Center of Excellence (CEGA)”. Lucy McGee is acknowledged for  
31 reviewing the English. Comments and suggestions from Dr. A. Inoue, Dr. J.

1 Moore and an anonymous referee strongly improved the previous version of the  
2 Ms.

3

#### 4 **References**

5 Abad, I., Mata, P., Nieto, F., Velilla, N., 2001. The phyllosilicates in diagenetic-  
6 metamorphic rocks of the South Portuguese Zone, southwestern Portugal.  
7 *Canadian Mineralogist* 39, 1571-1589. DOI: 10.2113/gscanmin.39.6.1571

8

9 Abad-Ortega, M.D., Nieto, F., 1995. Extension and closure of the compositional  
10 gap between Mn-rich and Mg-rich chlorites toward Fe-rich compositions.  
11 *European Journal of Mineralogy* 7, 363-367. DOI: 0935-1221/95/0007-036

12 3

13

14 Abad, I., Nieto, F., Gutiérrez-Alonso, G., 2003a. Textural and chemical changes  
15 in slate-forming phyllosilicates across the external-internal zones transition in the  
16 low-grade metamorphic belt of the NW Iberian Variscan Chain. *Schweizerische*  
17 *Mineralogische und Petrographische Mitteilungen* 83, 63-80. DOI: 10.5169/seals-  
18 63136

19

20 Abad, I., Nieto, F., Gutierrez-Alonso, G., Do Campo, M., Lopez-Munguira, A.,  
21 Velilla, N., 2006. Illitic substitution in micas of very low-grade metamorphic clastic  
22 rocks. *European Journal of Mineralogy* 18, 59-69. DOI: 10.1127/0935-  
23 1221/2006/0018-0059

24

25 Abad, I., Nieto, F., Peacor, D.R., Velilla, N., 2003b. Prograde and retrograde  
26 diagenetic and metamorphic evolution in metapelitic rocks of Sierra Espuña  
27 (Spain). *Clay Minerals* 38, 1-23. DOI: 10.1180/0009855033810074

28

29 Abid, I.A., Hesse, R., Harper, J.D., 2004. Variations in mixed-layer illite/smectite  
30 diagenesis in the rift and post-rift sediments of the Jeanne d'Arc Basin, Grand

1 Banks, offshore Newfoundland, Canada. *Canadian Journal of Earth Sciences* 41,  
2 401-429. DOI: 10.1139/E04-004  
3  
4 Aguirre, L., Robinson, D., Bevins, R.E., Morata, D., Vergara, M., Fonseca, E.,  
5 Carrasco, J., 2000. A low-grade metamorphic model for the Miocene volcanic  
6 sequences in the Andes of central Chile. *New Zealand Journal of Geology and*  
7 *Geophysics*, 43, 83-93. DOI: 10.1080/00288306.2000.9514871  
8  
9 Arcos, R., Charrier, R., Munizaga, F., 1988. Volcanitas cuaternarias en la hoya  
10 superior del Río Tinguiririca (34°40' Lat S – 70°21' Long W): características  
11 geológicas, antecedentes geoquímicos y geocronológicos. V Congreso  
12 Geológico Chileno, Tomo III, 1254-1260.  
13  
14 Árkai, P., Mata, M.P., Giorgetti, G., Peacor, D.R., Tóth, M., 2000. Comparison of  
15 diagenetic and low-grade metamorphic evolution of chlorite in associated  
16 metapelites and metabasites: an integrated TEM and XRD study. *Journal of*  
17 *Metamorphic Geology* 18, 531-550. DOI: 10.1046/j.1525-1314.2000.00272.x.  
18  
19 Árkai, P., Merriman, R.J., Roberts, B., Peacor, D.R., Tóth, M., 1996. Crystallinity,  
20 crystallite size and lattice strain of illite-muscovite and chlorite: Comparison of  
21 XRD and TEM data for diagenetic to epizonal pelites. *European Journal of*  
22 *Mineralogy* 8, 1119-1137.  
23  
24 Arostegui, J., Sangüesa, F.J., Nieto, F., Uriarte, J.A., 2006. Thermal models and  
25 clay diagenesis in the Tertiary-Cretaceous sediments of the Alava block (Basque-  
26 Cantabrian basin, Spain). *Clay Minerals* 41, 791-809. DOI:  
27 10.1180/0009855064140219  
28  
29 Bauluz, B., Peacor, D.R., Gonzalez-Lopez, J.M., 2000. Transmission electron  
30 microscopy study of illitization in pelites from the Iberian Range, Spain: layer-by-

1 layer replacement? *Clays and Clay Minerals* 48, 374-384. DOI:  
2 10.1346/CCMN.2000.0480308  
3  
4 Bauluz, B., Peacor, D.R, Ylagan, R.F., 2002. Transmission electron microscopy  
5 study of smectite illitization during hydrothermal alteration of a rhyolitic  
6 hyaloclastite from Ponza, Italy. *Clays and Clay Minerals* 50, 157-173. DOI:  
7 10.1346/000986002760832766.  
8  
9 Beaufort, D., Baronnet, A., Lanson, B., Meunier, A., 1997. Corrensite: A single  
10 phase or a mixed-layer phyllosilicate in the saponite-to-chlorite conversion  
11 series? A case study of Sancerre-Couy deep drill hole (France). *American*  
12 *mineralogist*, 82, 109-24.  
13  
14 Bettison, V., Mackinnon, J.D.R., Schiffman, P., 1991. Integrated TEM, XRD and  
15 electron microprobe investigation of mixed-layer chlorite-smectite from the Point  
16 Sal ophiolite, California. *Journal of Metamorphic Geology* 9, 697-710. DOI:  
17 0.1111/j.1525-1314.1991.tb00559.x  
18  
19 Bourdelle, F., Parra, T., Chopin, C., Beyssac, O., 2013. A new chlorite  
20 geothermometer for diagenetic to low-grade metamorphic conditions.  
21 *Contribution to Mineralogy and Petrology*, DOI 10.1007/s00410-012-0832-7.  
22  
23 Browne, P.R.L., 1978. Hydrothermal alteration in active geothermal fields. *Annual*  
24 *Reviews of Earth and Planetary Sciences* 6, 229-250.  
25  
26 Cathelineau, M., 1988. Cation site occupancy in chlorites and illites as a function  
27 of temperature. *Clay minerals* 23, 471-485. DOI: 10.1180/claymin.1988.023.4.13  
28  
29 Cathelineau, M., Nieva, D., 1985. A chlorite solid solution geothermometer. The  
30 Los Azufres (Mexico) geothermal system. *Contributions to Mineralogy and*  
31 *Petrology* 91, 235-247. DOI: 10.1007/BF00413350



1  
2 Clavero, J., Pineda, G., Mayorga, C., Giavelli, A., Aguirre, L., Simmons, S.,  
3 Martini, S., Soffia, J., Arriaza, R., Polanco, E., Achurra, L., 2011. Geological,  
4 geochemical, geophysical and first drilling data from Tinguiririca geothermal area,  
5 Central Chile. Geothermal Research Council Transactions. Vol. 35, 731-734.  
6  
7 Cliff, G., Lorimer, G.W., 1975. The quantitative analysis of thin specimens.  
8 Journal of Microscopy 103, 203-207.  
9  
10 de Caritat, P., Hutcheon, I., Walshe, J. L., 1993. Chlorite Geothermometry - A  
11 Review. Clays and Clay Minerals 41, 219-239. DOI:  
12 10.1346/CCMN.1993.0410210  
13  
14 Dong, H., Peacor, D.R., 1996. TEM observations of coherent stacking relations in  
15 smectite, I/S and illite of shales: evidence for MacEwan crystallites and  
16 dominance of 2M1 polytypism. Clays and Clay Minerals 44, 257-275.  
17 10.1346/CCMN.1996.0440211  
18  
19 Dong, H., Peacor, D.R., Freed, R.L., 1997. Phase relations among smectite, R1  
20 illite-smectite, and illite. American Mineralogist 82, 379-391.  
21  
22 Droguett, B., Morata, D., Clavero, J., Pineda, G., Morales, S., Carrillo, F.J., 2012.  
23 Mineralogía de alteración en el pozo Pte-1, campo geotermal Tinguiririca, Chile.  
24 Congreso Geologico Chile-2012.  
25  
26 Essene, E.J., Peacor D.R., 1995. Clay mineral thermometry. A critical  
27 perspective. Clays and Clay Minerals 43, 540-549. DOI:  
28 10.1346/CCMN.1995.0430504  
29  
30 Ferrage, E., Vidal, O, Mosser-Ruck, R, Cathelinea, M., Cuadros, J., 2011. A  
31 reinvestigation of smectite illitization in experimental hydrothermal conditions:

1 Results from X-ray diffraction and transmission electron microscopy. *American*  
2 *Mineralogist* 96, 207-223. DOI: 10.2138/am.2011.3945. 1903.  
3  
4 Fuentes, F. Aguirre, L., Vergara, M., Valdebenito, L., Fonseca, E., 2004. Miocene  
5 fossil hydrothermal system associated with a volcanic complex in the Andes of  
6 central Chile. *Journal of Volcanology and Geothermal Research*, 138, 139-161.  
7 DOI: 10.1016/j.jvolgeores.2004.07.001.  
8  
9 Giorgetti, G., Mata, P., Peacor, D.R., 2000. TEM study of the mechanism of  
10 transformation of detrital kaolinite and muscovite to illite/smectite in sediments of  
11 the Salton Sea geothermal field. *European Journal of Mineralogy* 12, 923-934.  
12 10.1127/0935-1221/2000/0012-0923.  
13  
14 Giorgetti, G., Mata, M.P., Peacor, D.R., 2003. Evolution of mineral assemblages  
15 and textures from sediment through hornfels in the Salton Sea geothermal field:  
16 Direct crystallization of phyllosilicates in a hydrothermal-metamorphic system.  
17 *Clay Minerals* 38, 113-126. DOI: 10.1180/0009855033810082  
18  
19 Grim, R.E., Güven, N., 1978. *Bentonites: Geology, Mineralogy, Properties and*  
20 *Uses*. Elsevier, Amsterdam, The Netherlands.  
21  
22 Guisseau, D., Patrier-Mas, P., Beaufort, D., Girard, J.P., Inoue, A., Sanjuan, B.,  
23 Petit, S., Lens, A., Genter, A., 2007. Significance of the depth-related transition  
24 montmorillonite-beidellite in the Bouillante geothermal field (Guadeloupe, Lesser  
25 Antilles). *American Mineralogist* 92, 1800-1813. DOI: 10.2138/am.2007.2398.  
26  
27 Guthrie, G.D., Veblen, D.R., 1989a. High-resolution transmission electron  
28 microscopy of mixed-layer illite/ smectite: Computer simulations. *Clays and Clay*  
29 *Minerals* 37, 1-11. DOI: 10.1346/CCMN.1989.0370101.  
30

1 Guthrie, G.D., Veblen, D.R., 1989b. High-resolution transmission electron  
2 microscopy applied to clay minerals. In Spectroscopic Characterization of  
3 Minerals and their Surfaces (L.M. Coyne, S.W.S. McKeever and D.F. Blake,  
4 editors). Symposia Series 415, American Chemical Society, Washington, D.C.  
5  
6 Guthrie, G.D., Veblen, D.R., 1990. Interpreting one- dimensional high-resolution  
7 transmission electron micrographs of sheet silicates by computer simulation.  
8 American Mineralogist 75, 276-288.  
9  
10 Guthrie, GD., Reynolds, RC., 1998. A coherent TEM- and XRD-description of  
11 mixed-layer illite/smectite. Canadian Mineralogist 36, 1421-1434.  
12  
13 Güven, N., Grim, R., 1972. X-ray diffraction and electron optical studies on  
14 smectite and a-cristobalite associations. Clays and Clay Minerals 20, 89-92.  
15  
16 Harvey, C.C., Browne, P.R.L., 1991. Mixed-layer clay geothermometry in the  
17 Wairakei geothermal field, New Zealand. Clays and Clay Minerals 39, 614-621.  
18 DOI: 10.1346/CCMN.1991.0390607  
19  
20 Hay, R.L., Sheppard, R.A., 2001. Occurrence of zeolites in sedimentary rocks:  
21 An overview. Pp. 217 – 234 in: Natural Zeolites: Occurrence, Properties,  
22 Applications (D.L. Bish and D.W. Ming, editors). Reviews in Mineralogy and  
23 Geochemistry, 45. Mineralogical Society of America, Washington, D.C.  
24  
25 Henley, R.W., Ellis, A.J., 1983. Geothermal systems ancient and modern: a  
26 geochemical review. Earth Science Reviews 19, 1-50.  
27  
28 Hoffman, J., Hower, J., 1979. Clay mineral assemblages as low grade  
29 metamorphic geothermometers: Application to the thrust-faulted disturbed belt of  
30 Montana, U.S.A.: in Aspects of Diagenesis, P. A. Scholle and P. R. Schluger,

1 eds., Society Economic Palaeontologists and Mineralogist Special Publication.  
2 26, 55-79.  
3  
4 Inoue, A., Meunier, A., Beaufort, D., 2004. Illite-Smectite Mixed-Layer Minerals In  
5 Felsic Volcaniclastic Rocks From Drill Cores, Kakkonda, Japan. *Clays and Clay*  
6 *Minerals* 52, 66-84. DOI: 10.1346/CCMN.2004.0520108.  
7  
8 Inoue, A., Meunier, A., Patrier-Mas, P., Rigault, C., Beaufort, D., Vieillard, P.,  
9 2009. Application of chemical geothermometry to low-temperature trioctahedral  
10 chlorites. *Clays and Clay Minerals* 57, 371-382.  
11 DOI:10.1346/CCMN.2009.0570309.  
12  
13 Inoue, A., Utada, M., 1991. Smectite-to-chlorite transformation in thermally  
14 metamorphosed volcanoclastic rocks in the Kamikita area, northern Honshu,  
15 Japan. *American Mineralogist* 76, 628-640.  
16  
17 Inoue, A., Utada, M., Nagata, H., Watanabe, T., 1984. Conversion of  
18 trioctahedral smectite to interstratified chlorite/smectite in Pliocene acidic  
19 pyroclastic sediments of the Ohyu district, Akita Prefecture, Japan: *Clay Science*,  
20 6, 103-106.  
21  
22 Ji, J., Browne, P.R.L., 2000. Relationship between illite crystallinity and  
23 temperature in active geothermal systems of New Zealand. *Clays and Clay*  
24 *Minerals* 48, 139. DOI: 10.1346/CCMN.2000.0480117  
25  
26 Keith, T.E.C., Bargar, I.C.E., 1988. Petrology and hydrothermal mineralogy  
27 of U.S. Geological Survey Newberry 2 drill core from Newberry  
28 caldera, Oregon. *Journal of Geophysical Research* 93, 10174-10190.  
29  
30 Kim, J.W., Peacor, D.R., Tessier, D., Elsass, F., 1995. A technique for  
31 maintaining texture and permanent expansion of smectite interlayers for TEM

1 observations. *Clays and Clay Minerals* 43, 51-57. DOI:  
2 10.1346/CCMN.1995.0430106  
3  
4 Kogure, T., Drits, V.A, Inoue, S., 2013. Structure of mixed-layer corrensite-  
5 chlorite revealed by high-resolution transmission electron microscopy (HRTEM).  
6 *American Mineralogist* 98, 1253-1260. DOI: 10.2138/am.2013.4314. 1253  
7  
8 Kristmannsdótti, H., 1976. Types of clay minerals in hydrothermally altered  
9 basaltic rocks, Reykjanes, Iceland: *Jokull* 26, 30-39.  
10  
11 Leoni, L., Lezzerini, M., Battaglia, S., Cavalcante, E., 2010. Corrensite and  
12 chlorite-rich Chl-S mixed layers in sandstones from the 'Macigno' Formation  
13 (northwestern Tuscany, Italy). *Clay Minerals* 45, 87-106. DOI:  
14 10.1180/claymin.2010.045.1.87  
15  
16 Libbey, R.B., Longstaffe, F.J., Flemming, R.L., 2013. Clay mineralogy, oxygen  
17 isotope geochemistry, and water/rock ratio estimates, Te Mihi area, Wairakei  
18 geothermal field, New Zealand. *Clays and Clay Minerals* 61, 204-217. DOI:  
19 10.1346/CCMN.2013.0610304  
20  
21 Lindgreen, H., 1991. Elemental and structural changes in illite/smectite mixed-  
22 layer clay minerals during diagenesis in Kimmeridgian- Volgian(-Ryazanian)  
23 clays in the Central Trough, North Sea and the Norwegian-Danish Basin. *Bulletin*  
24 *of the Geological Society of Denmark* 39, 1-82.  
25  
26 Lopez-Munguira, A., Nieto, F., Morata, D., 2002. Chlorite composition and  
27 geothermometry: a comparative HRTEM/AEM-EMPA-XRD study of Cambrian  
28 basic lavas from the Ossa Morena Zone, SW Spain. *Clay Minerals* 37, 267-281.  
29 DOI: 10.1180/0009855023720033  
30

1 McDowell, S.D., Elders, W.A., 1980. Auriferous layer silicate minerals in  
2 borehole Elmore #1, Salton Sea geothermal field, California, USA. Contributions  
3 to Mineralogy and Petrology 74, 293-310. DOI: 10.1007/s004100050163  
4

5 Mas, A., Guisseau, D., Patrier, P., Beaufort, D., Genter, A., Sanjuan, B., Girard,  
6 J.P., 2006. Clay minerals related to the hydrothermal activity of the Bouillante  
7 geothermal field (Guadeloupe). Journal of Volcanology and Geothermal  
8 Research 158, 380-400. DOI: 10.1016/j.jvolgeores.2006.07.010  
9

10 Mas, A., Patrier, P., Beaufort, D., Genter, A., 2003. Clay-mineral signatures of  
11 fossil and active hydrothermal circulations in the geothermal system of the  
12 Lamentin Plain, Martinique. Journal of Volcanology and Geothermal Research  
13 124, 195-218. DOI: 10.1016/S0377-0273(03)00044-1  
14

15 Merriman, R.J., Peacor, D.R., 1999. Very low-grade metapelites; mineralogy,  
16 microfabrics and measuring reaction progress. Pp. 10-60 in: Low-Grade  
17 Metamorphism (M. Frey & D. Robinson, editors). Blackwell Sciences Ltd.,  
18 Oxford, UK.  
19

20 Merriman, R.J., Roberts, B., Peacor, D.R., Hirons, S.R., 1995. Strain-related  
21 differences in the crystal-growth of white mica and chlorite - a TEM and XRD  
22 study of the development of metapelitic microfabrics in the southern uplands  
23 thrust terrane, Scotland. Journal of Metamorphic Geology 13, 559-576. DOI:  
24 10.1111/j.1525-1314.1995.tb00243.x  
25

26 Meunier, A., Inoue, A., Beaufort, D., 1991. Chemigraphic analysis of  
27 trioctahedral smectite-to-chlorite conversion series from The Ohyu Caldera,  
28 Japan. Clays and Clay Minerals 39, 409-415. DOI:  
29 10.1346/CCMN.1991.0390410  
30

1 Meunier, A., Mas, A., Beaufort, D., Patrier, P., Dudoignon, P., 2008a. Clay  
2 minerals in basalt-hawaiite rocks from Mururoa atoll (French Polynesia). I.  
3 Mineralogy. *Clays and Clay Minerals* 56, 711-729. DOI:  
4 10.1346/CCMN.2008.0560611  
5  
6 Meunier, A., Mas, A., Beaufort, D., Patrier, P., Dudoignon, P., 2008b. Clay  
7 minerals in basalt-hawaiite rocks from Mururoa atoll (French Polynesia). II.  
8 Petrography and geochemistry. *Clays and Clay Minerals* 56, 730-750. DOI:  
9 10.1346/CCMN.2008.0560612  
10  
11 Meunier, A., Velde, B., 1989. Solid solution in illite/smectite mixed layer minerals  
12 and illite. *American Mineralogist* 74, 1106-1112.  
13  
14 Moore, D.M., Reynolds, R.C., Jr., 1997. X-ray diffraction and the Identification  
15 and Analysis of Clay Minerals, 2nd edition. Oxford University Press, New York,  
16 pp. 227-296.  
17  
18 Morse, J.W., Casey, W.H., 1988. Ostwald processes and mineral paragenesis in  
19 sediments *American Journal of Science* 288, 537-560.  
20  
21 Muffler, L.P.J., White, D.E., 1969. Active metamorphism of Upper Cenozoic  
22 sediments in the Salton Sea geothermal field and the Salton Trough,  
23 southeastern California. *Geological Society of America Bulletin* 80, 157-182.  
24  
25 Nieto, F., Ortega-Huertas, M., Peacor, D.R., Aróstegui, J., 1996. Evolution of  
26 illite/smectite from early diagenesis through incipient metamorphism in sediments  
27 of the Basque-Cantabrian basin. *Clays and Clay Minerals* 44, 304-323. DOI:  
28 10.1346/CCMN.1996.0440302  
29

1 Pollastro, R.M., 1993. Considerations and applications of the illite/ smectite  
2 geothermometer in hydrocarbon-bearing rocks of Miocene to Mississippian Age.  
3 *Clays and Clay Minerals* 41, 119-133. DOI: 10.1029/2000JB000027.  
4

5 Reyes, A.G., 1990. Petrology of Philippine geothermal systems and the  
6 application of alteration mineralogy to their assessment. *Journal of Volcanology  
7 and Geothermal Research* 43, 279-309. DOI: 10.1016/0377-0273(90)90057-M  
8

9 Robinson, D., Bevins, R.E., 1994. Mafic phyllosilicates in low-grade metabasites.  
10 Characterization using deconvolution analysis. *Clay Minerals* 29, 223-237. DOI:  
11 10.1180/claymin.1994.029.2.08  
12

13 Schegg, R., Leu, W., 1996. Clay mineral diagenesis and thermal history of the  
14 Thonex Well, Western Swiss Molasse Basin. *Clays and Clay Minerals* 44, 693-  
15 705. DOI: 10.1346/CCMN.1996.0440513  
16

17 Schiffman, P., Fridleifsson, G.O., 1991. The smectite to chlorite transition in  
18 drillhole NJ-15, Nesjavellir geothermal field, Iceland: XRD, BSE and electron  
19 microprobe investigations. *Journal of Metamorphic Geology* 9, 679-696. DOI:  
20 10.1111/j.1525-1314.1991.tb00558.x.  
21

22 Schiffman, P., Staudigel, H., 1995. Hydrothermal alteration of a seamount  
23 complex on La Palma, Canary Islands: implications for metamorphism in  
24 accreted terranes. *Geology* 22, 151-54. DOI: 10.1130/0091-  
25 7613(1994)022<0151:HAOASC>2.3.CO;2  
26

27 Schmidt, S.Th., Robinson, D., 1997. Metamorphic grade and porosity and  
28 permeability controls on mafic phyllosilicate distributions in a regional zeolite to  
29 greenschist facies transition of the North Shore Volcanic Group, Minnesota. *GSA  
30 Bulletin* 109, 683-697.  
31



1 Shau, Y.H., Peacor, D.R., Essene, E.J., 1990. Corrensite and mixed-layer  
2 chlorite/smectite in metabasalt from northern Taiwan: TEM/AEM, EMPA, XRD,  
3 and optical studies. *Contributions to Mineralogy and Petrology* 105, 123-142.  
4 DOI: 10.1007/BF00678980  
5

6 Shau, Y.H., Peacor, D.R., 1992. Phyllosilicates in hydrothermally altered basalts  
7 from DSDP hole 504b, leg-83 - a TEM and AEM study. *Contributions to*  
8 *Mineralogy and Petrology* 112, 119-133. DOI: 10.1007/BF00310959  
9

10 Srodon, J., Eberl, D.D., 1984. Illite. Pp. 495-544 in: *Micas* (S.W. Bailey, editor).  
11 *Reviews in Mineralogy*, 13. Mineralogical Society of America, Washington D.C.,  
12 USA.  
13

14 Uysal, I.T., Glikson, M., Golding, S.D., Audsley, F., 2000. The thermal history of  
15 the Bowen Basin, Queensland, Australia: vitrinite reflectance and the clay  
16 mineralogy of Late Permian coal measures. *Tectonophysics* 323, 105-129. DOI:  
17 10.1016/S0040-1951(00)00098-6  
18

19 Veblen, D.R., Guthrie, G.D., Livi, K.J.T., Reynolds, R.C. Jr., 1990. High-  
20 resolution transmission electron microscopy and electron diffraction of mixed-  
21 layer illite/smectite: Experimental results. *Clays and Clay Minerals* 38, 1-13. DOI:  
22 10.1346/CCMN.1990.0380101  
23

24 Velde, B., 1985. *Clay Minerals: a Physico-Chemical Explanation of their*  
25 *Ocurrence*. Elsevier, Amsterdam y New York.  
26

27 Vergara, M., Levi, B., Villaroel, R., 1993. Geothermal-type alteration in a burial  
28 metamorphosed volcanic pile, central Chile. *Journal of Metamorphic Geology* 11,  
29 449-454. DOI: 10.1111/j.1525-1314.1993.tb00161.x  
30

1 Vidal, O., De Andrade, V., Lewin, E., Munoz, M., Parra, T., Pascarelli, S., 2006.  
2 P-T-deformation-Fe<sup>3+</sup>/Fe<sup>2+</sup> mapping at the thin section scale and comparison  
3 with XANES mapping: application to a garnet-bearing metapelite from the  
4 Sambagawa metamorphic belt (Japan). *Journal of Metamorphic Geology* 24,  
5 669-683. DOI: 10.1111/j.1525-1314.2006.00661.x  
6  
7 Vidal, O., Parra, T., Vieillard, P., 2005. Thermodynamic properties of the  
8 Tschermak solid solution in Fe-chlorite: Application to natural examples and  
9 possible role of oxidation. *American Mineralogist* 90, 347-358. DOI:  
10 10.2138/am.2005.1554.  
11  
12 Warr, L.N., Nieto, F., 1998. Crystallite thickness and defect density of  
13 phyllosilicates in low-temperature metamorphic pelites: a TEM and XRD study of  
14 clay-minerals crystallinity-index standards. *Canadian Mineralogy* 36, 1453-1474.  
15  
16 Weaver, C.E., 1989. *Clays, muds, and shales. Development in Sedimentology*  
17 44, Elsevier, New York.  
18  
19 Wiewióra, A., Weiss, Z., 1990. Crystallochemical classifications of phyllosilicates  
20 based on the unified system of projection of chemical composition: II The chlorite  
21 group. *Clay Minerals* 25, 83-92. DOI: 10.1180/claymin.1990.025.1.09  
22  
23 Yau, Y.C., Peacor, D.R., Essene, E.J., 1987a. Authigenic anatase and titanite in  
24 shales from the Salton Sea geothermal field, California. *Neues Jahrbuch für*  
25 *Mineralogie Monatshefte*, 441-452.  
26  
27 Yau, Y.C., Peacor, D.R., McDowell, S.D., 1987b. Smectite-to-illite reactions in  
28 Salton Sea shales: a transmission and analytical electron microscopy study.  
29 *Journal of Sedimentary Petrology* 57, 335-342.  
30

1 Yau, Y.C., Peacor, D.R., Beane, R.E., Essene, E.J., McDowell, S.D., 1988.  
2 Microstructures, formation mechanism, and depth-zoning of phyllosilicates in  
3 geothermally altered shales, Salton Sea, California. *Clays and Clay Minerals* 36,  
4 1-10.

5

## 6 **Figure captions**

7

8 Fig. 1. Geological map of Tinguiririca geothermal field simplified from Clavero et  
9 al. (2011).

10

11 Fig. 2. Lithology and distribution of secondary minerals determined by Droguet et  
12 al. (2012) in PTe-1. Clay minerals distribution is also plotted according to their  
13 sampling depth. The values of temperature calculated by Bourdelle (2013)  
14 geothermometer, using chlorite composition presented on Table 2, are shown. I-  
15 S: Illite-smectite minerals; R= I-S Ordering; HC-Corr: High-charge corrensite; LC-  
16 Corr: Low-charge corrensite; C-V: chlorite-vermiculite mixed layers.

17

18 Fig. 3. Optical photomicrograph of the samples of Pte-1 borehole. (a)  
19 Porphyroblasts of plagioclase (Pl) partially replaced by phyllosilicates (Phy) and  
20 vesicle (Vs) are present in 158 sample. (b) Phyllosilicates filling voids in 262  
21 sample. (c) Prehenite (Prh) and quartz, adjacent to silica phase in 595 sample.  
22 (d) Crossed-nicols image of (c). (e) Phyllosilicates filling pores and as main  
23 constituent of the matrix in 699 sample. (f) Epidote (Ep) and Prehenite (Prh) are  
24 present as secondary minerals in 786 sample.

25

26 Fig. 4. XRD diagrams of the mixed layered clay minerals (a) Illite-Smectite (I-S)  
27 with 70% of illite and R1 ordering and low-charge corrensite in 328 sample, air-  
28 dried, EG solvated and heated to 300°C. (c) Low-charge corrensite in 786  
29 sample, air dried, EG solvated and heated to 300°C.

30

1 Fig. 5. Textural images of clay minerals. (a) Smectite (Sm) filling voids of  
2 plagioclase (Pl) in 158 sample. (b) HAADF image of I-S mixed layers showing  
3 curved and lens-shaped morphology and no preferred orientation in 328 sample.  
4 (c) Volcanic glass (VG) transformed to I-S mixed layers, quartz (Qtz) and  
5 plagioclase in 328 sample. (d) Low-charge corrensite filling irregular cavities of  
6 plagioclase in 776 sample.

7

8 Fig. 6. Smectite in 158 sample. (a) Smectite with lens-shaped morphology. (b)  
9 Discontinuous and wavy fringes of smectite with two families of d-spacings at 10  
10 and 4.5 Å.

11

12 Fig. 7. Clays mixed layers in 328 sample. (a) Illite-Smectite (I-S) mixed layers  
13 show curved small packets. Non-00l reflections are ill-defined, non-periodic and  
14 diffuse parallel to  $c^*$ , implying that stacking is generally random. Such SAED  
15 patterns are typical of 1M<sub>d</sub> polytypism. (b) The fringes have spacing (22 to 35 Å  
16 periodicity) characteristic of the sum of illite- and smectite-like layer spacings in  
17 (R=1) I-S. (c) and (d) Chlorite intergrowth and/or interstratified with 10 Å and 7 Å  
18 layers.

19

20 Fig. 8. High magnification images of clay minerals in 653 sample. (a) Illite  
21 showing lattice fringes with spacing to 10 Å. SAED pattern corresponds to 1M<sub>d</sub>  
22 polytypism. (b) Lattice fringes with spacing of 10 and 20 Å and SAED pattern  
23 corresponding to 2M polytypism in more mature mica. (c) Chlorite with 14 Å  
24 layers in 653 sample. SAED pattern corresponds to disordered chlorite polytype.

25

26 Fig. 9. Chlorite and low-charge corrensite in 776 sample. (a) Layers to 24 Å  
27 corresponding to corrensite, are the result of an ordered sum of one chlorite layer  
28 (14 Å) and one contracted smectite layer (10 Å). They are intergrowth with 14 Å  
29 chlorite layers and 20 Å of illite layers (2M polytype). (b) Layers to 14Å with minor  
30 10Å layers showing chlorite intergrowth and/or interstratified with corrensite.

31

1 Fig. 10. Compositional diagram of AEM analyses corresponding to smectite, and  
2 I-S mixed layers from 158, 328 and 653 samples. (a) Mg vs Fe. (b) Si vs  
3 Interlayer cations. (c) Si vs Mg. (d) Si vs K.

4  
5 Fig. 11. Compositional diagram MR<sup>3+</sup>- 2R<sup>3+</sup>-3R<sup>2+</sup> (Velde ,1985) of the smectite and  
6 I-S mixed layers AEM analysis. MR<sup>3+</sup>: (Na<sup>+</sup> + K<sup>+</sup> + 2Ca<sup>2+</sup>), 2R<sup>3+</sup>: (Al<sup>3+</sup> + Fe<sup>3+</sup>  
7 - MR<sup>3+</sup>)/2, 3R<sup>2+</sup>: (Fe<sup>2+</sup> + Mg<sup>2+</sup> + Mn<sup>2+</sup>)/3.

8  
9 Fig. 12. Compositional diagrams M<sup>+</sup>-4Si-3R<sup>2+</sup> (Meunier and Velde, 1989) of  
10 chlorite, corrensite and intermediate mixed layers of C-S and C-V (more than  
11 50% of chlorite). Theoretical chlorite composition is given by green line and  
12 theoretical 50-50 corrensite composition is plotted by black line (Meunier et. al,  
13 1991). M<sup>+</sup>= Na<sup>+</sup>, K<sup>+</sup>, 2Ca<sup>2+</sup>; 4Si= Si/4; 3R<sup>2+</sup>=(Mg<sup>2+</sup>+Fe<sup>2+</sup>+Mn<sup>3+</sup>)/3

14  
15 Fig. 13. Chemical compositions of chlorites from Tinguiririca geothermal field  
16 plotted in the R<sup>2+</sup>-Si diagram of Wiewióra and Weiss (1990); all Fe considered  
17 as Fe(II).

18

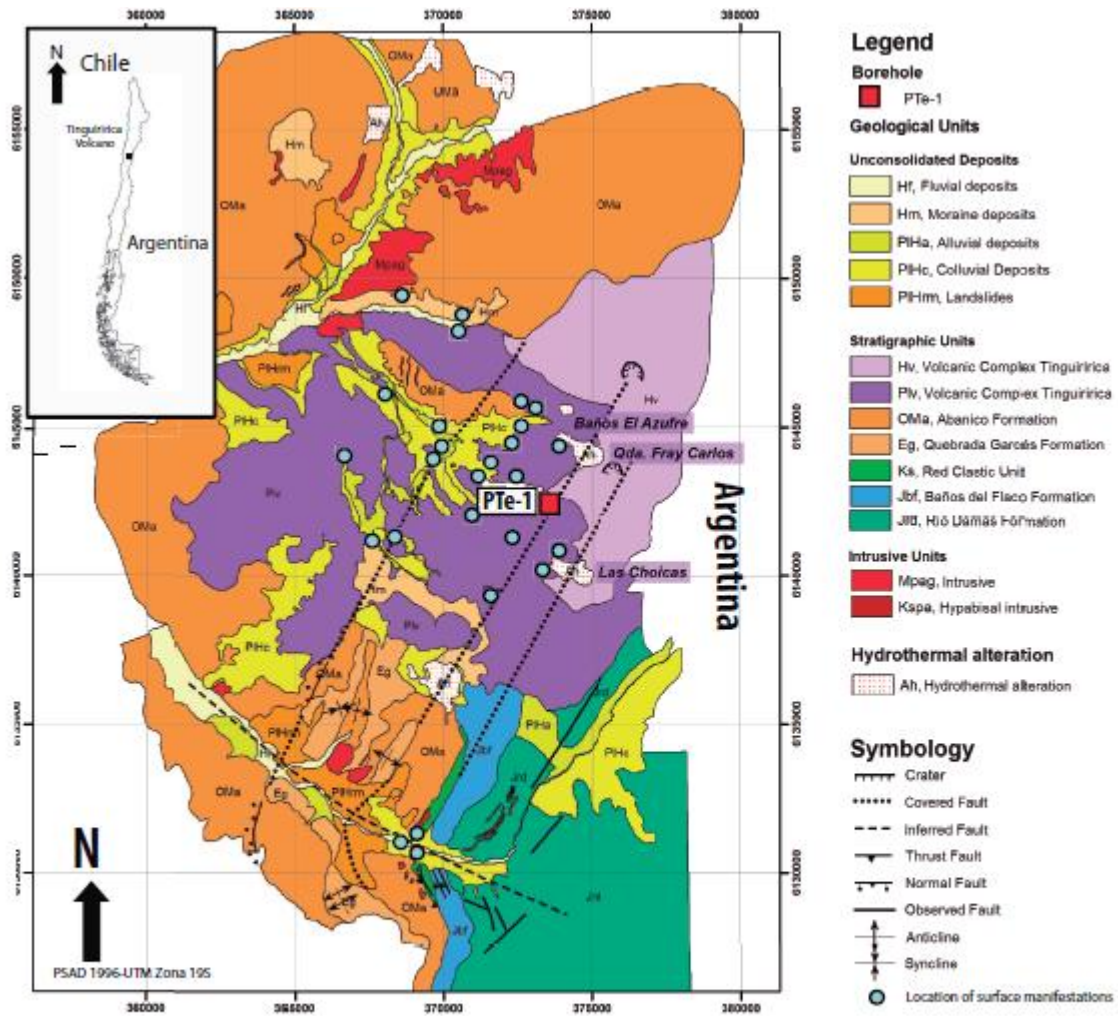


Fig.1

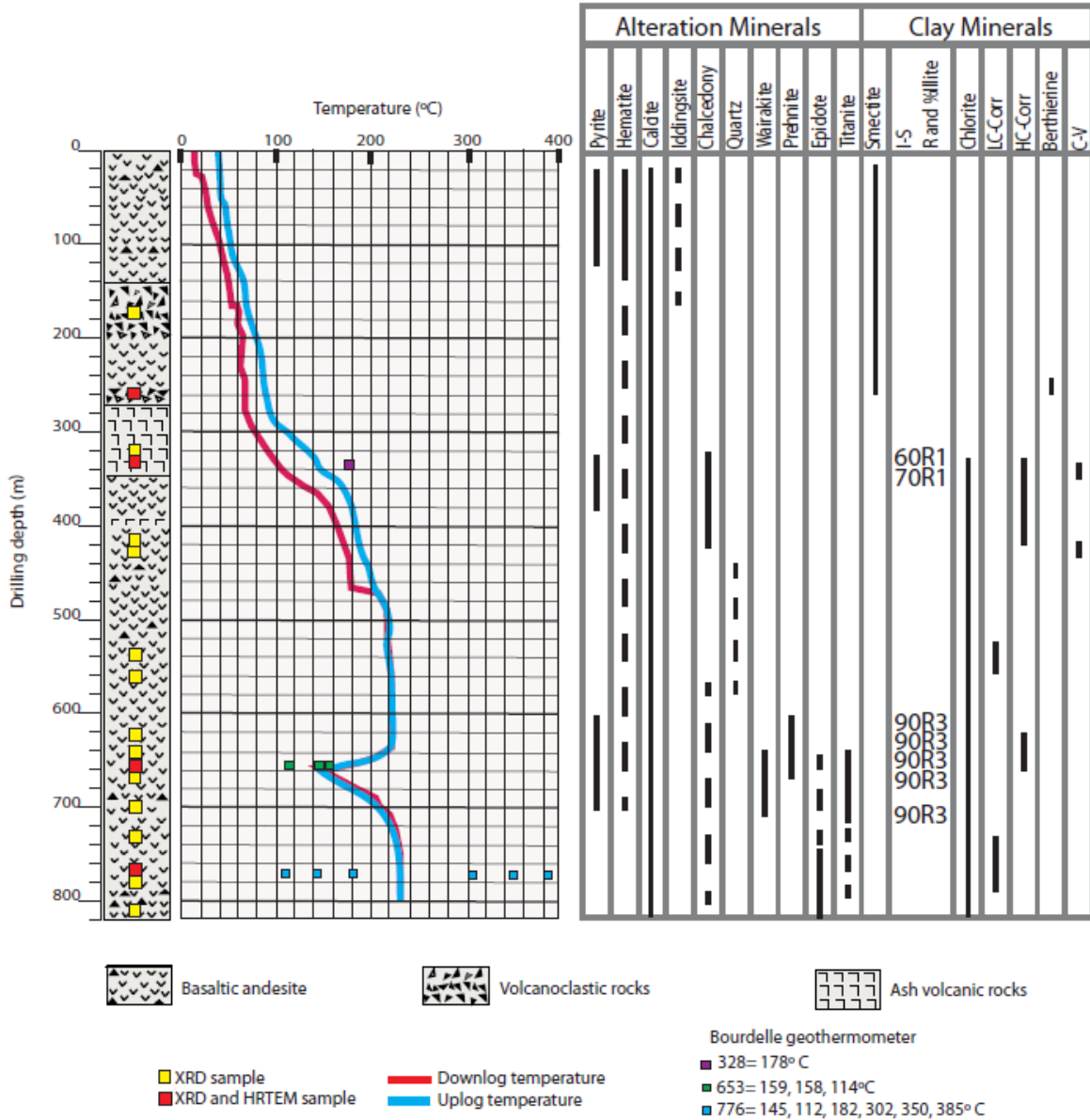


Fig. 2



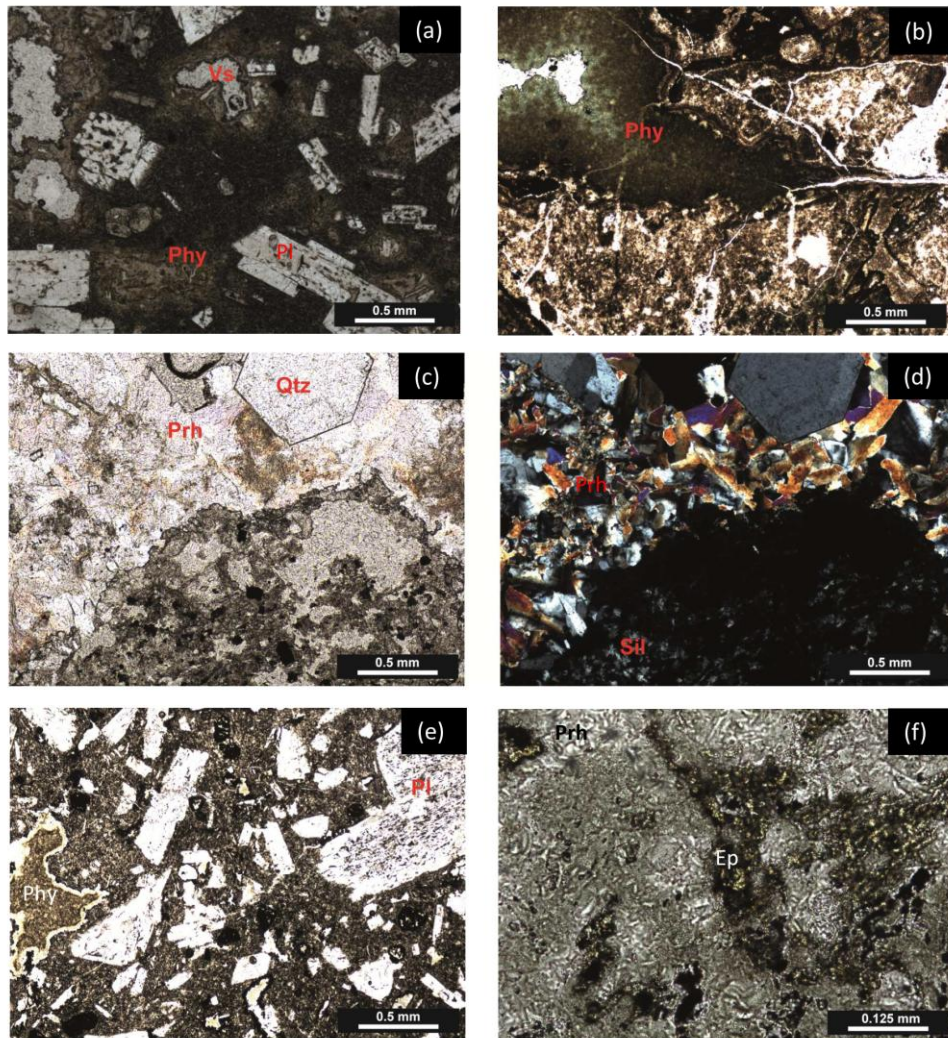


Fig. 3.



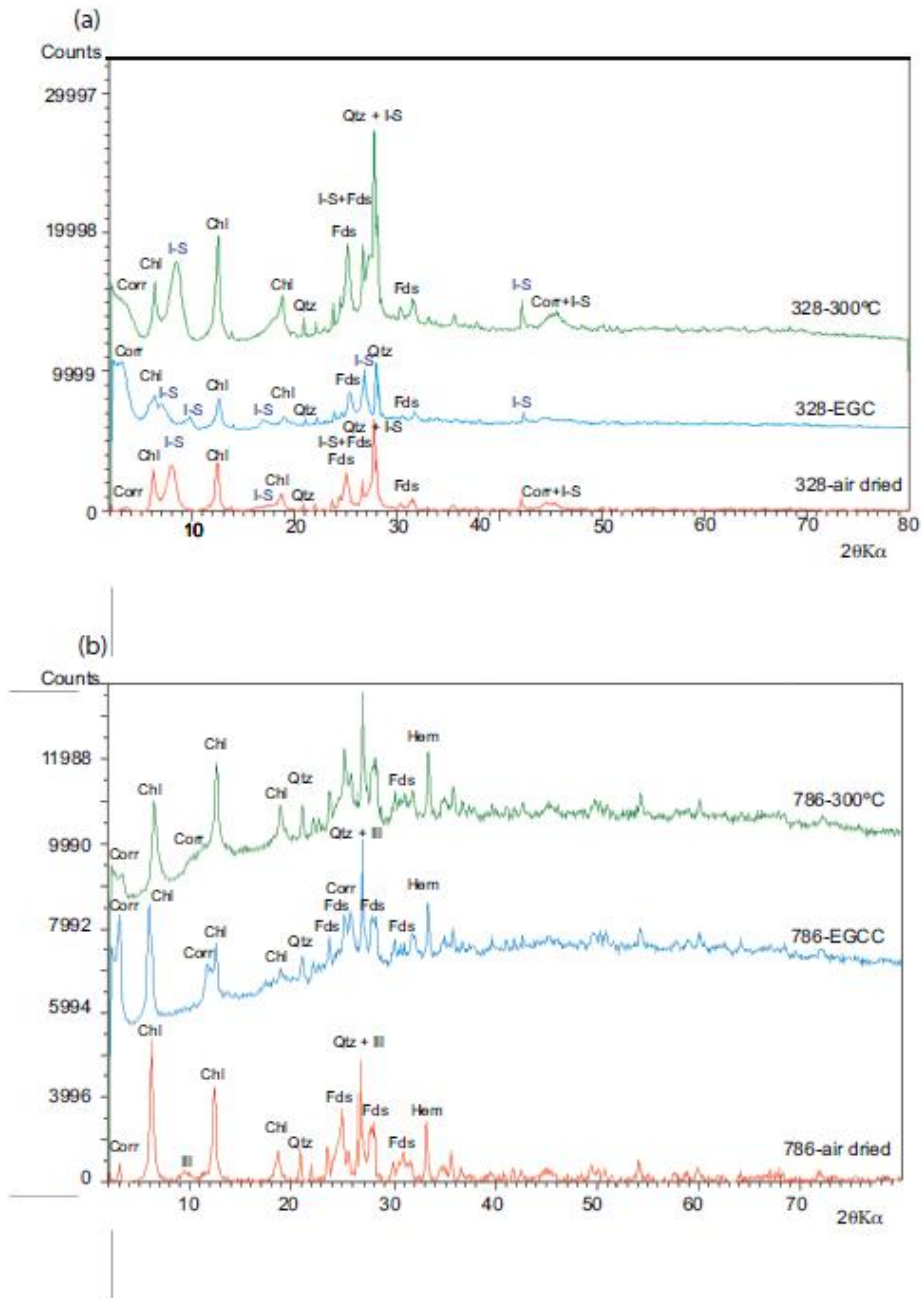


Figure 4

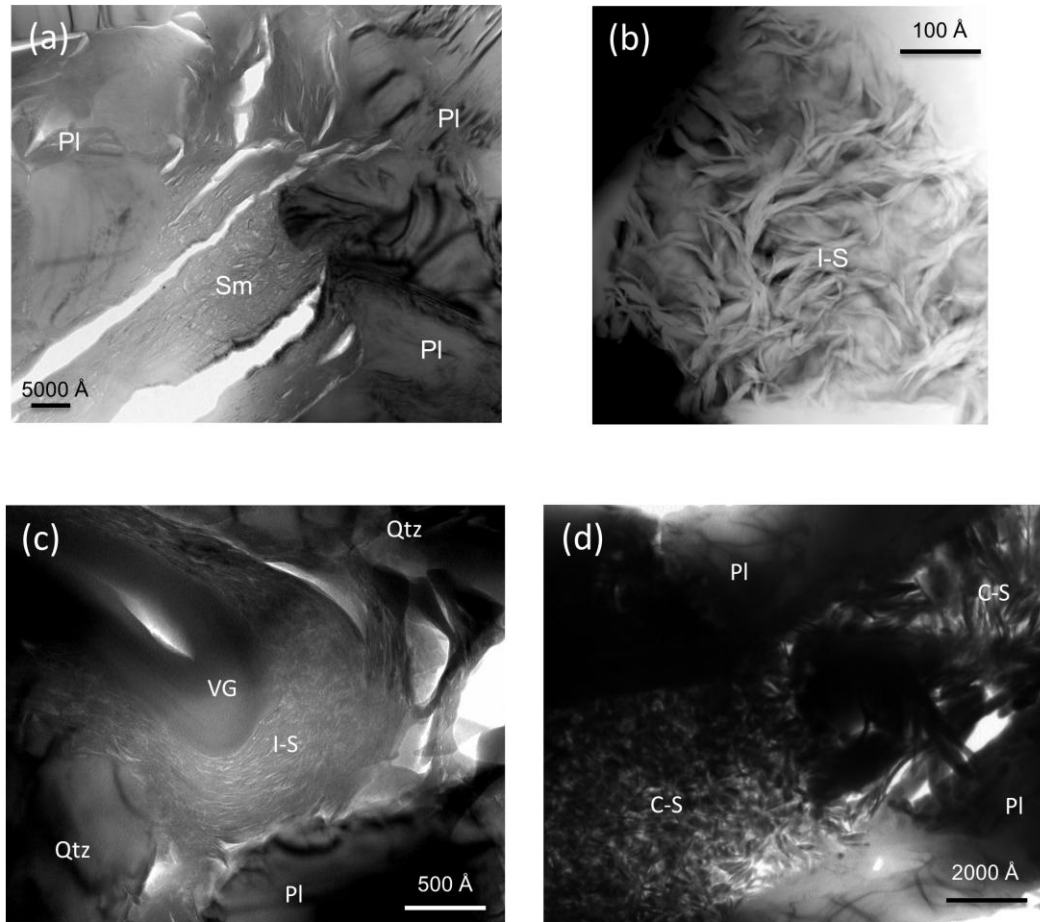


Fig. 5.

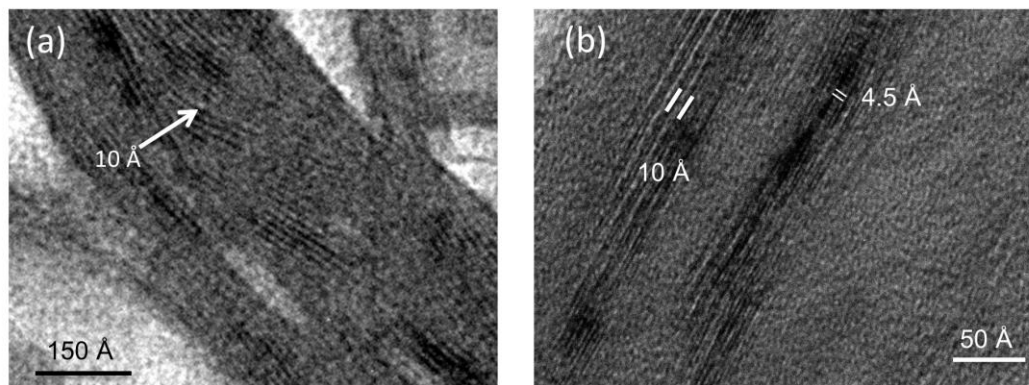


Fig. 6.

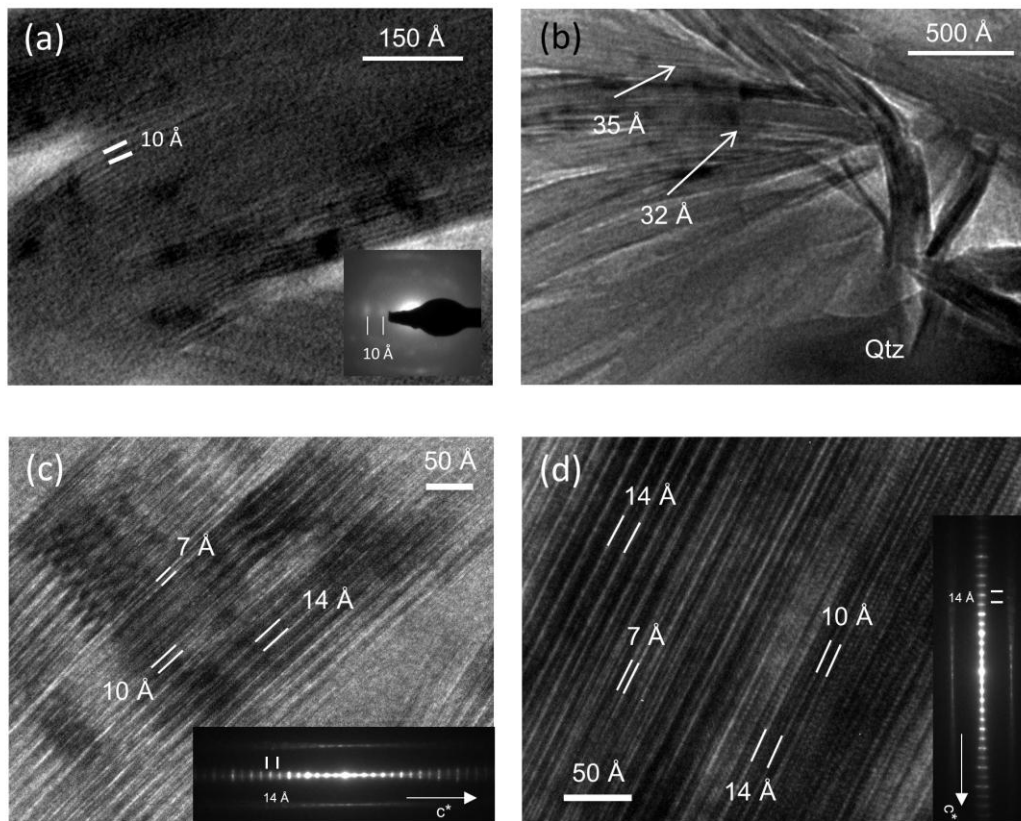


Fig. 7.

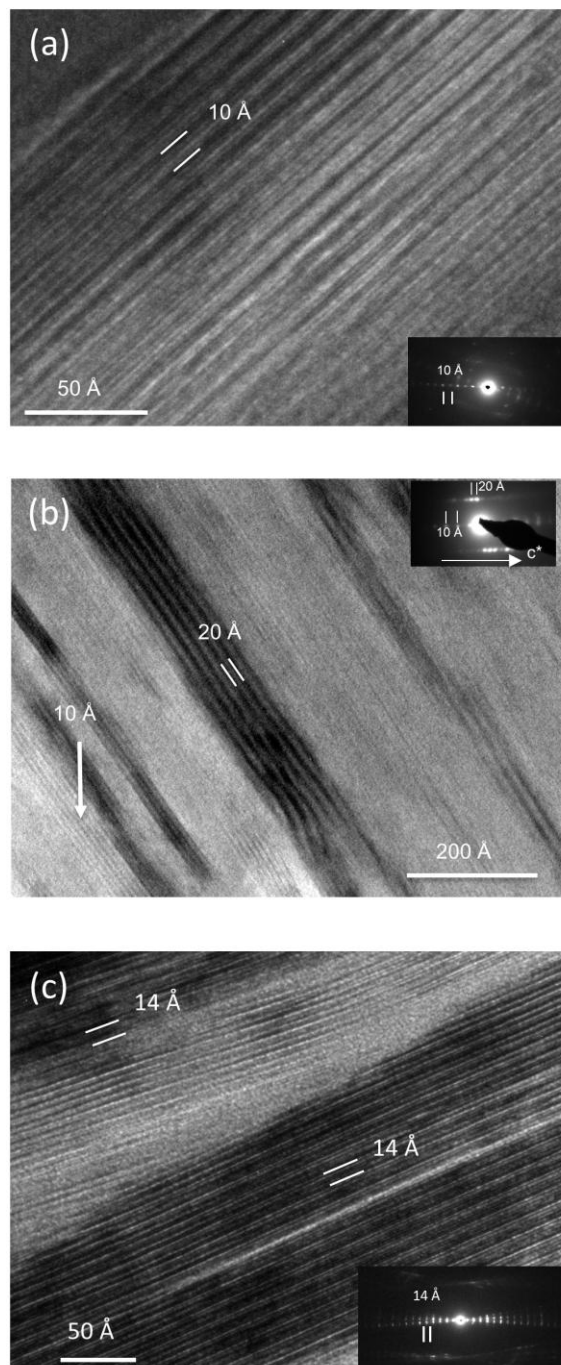


Fig. 8.

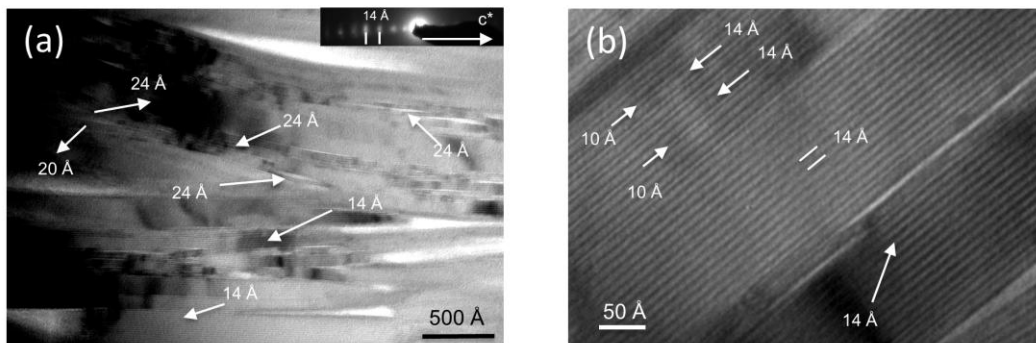


Fig. 9.

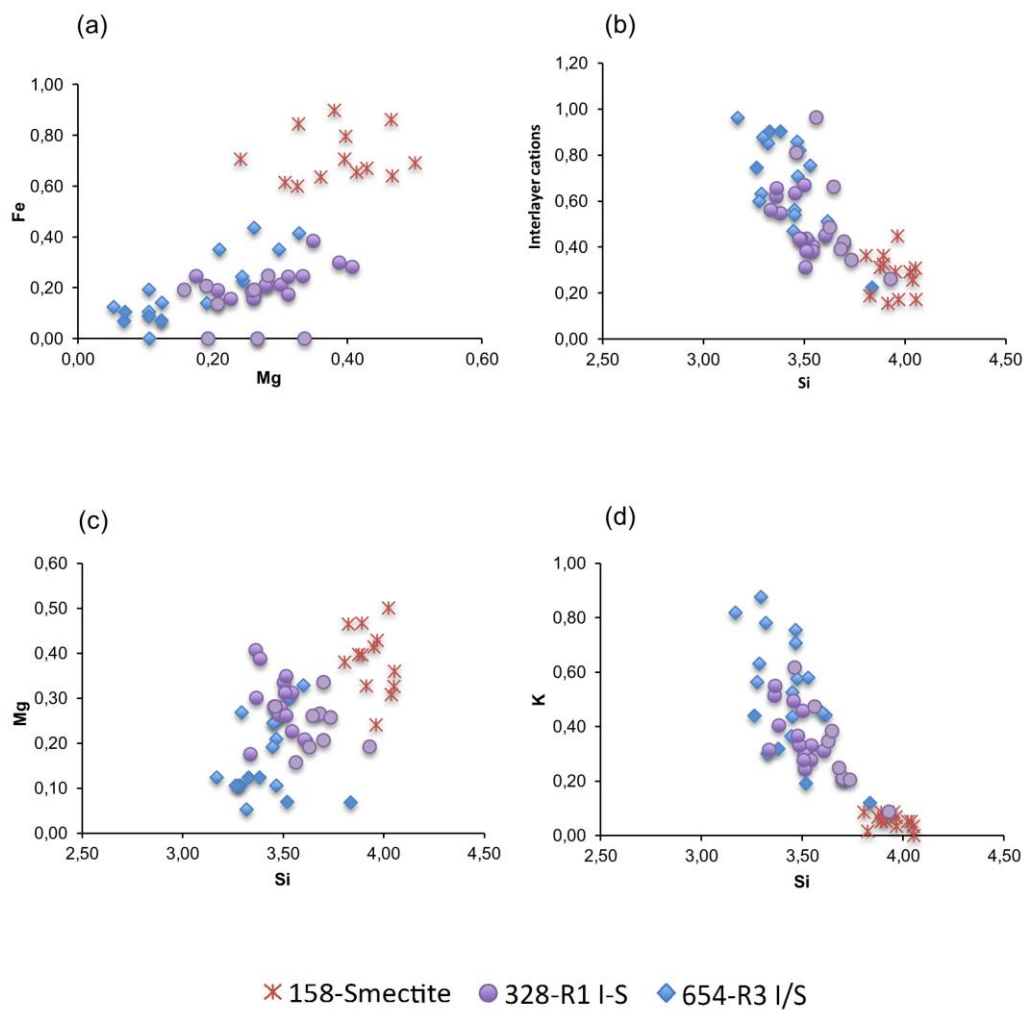


Fig. 10.

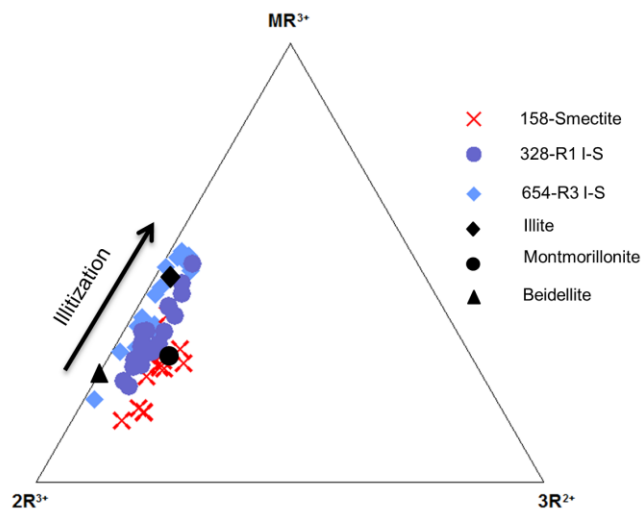


Fig. 11.



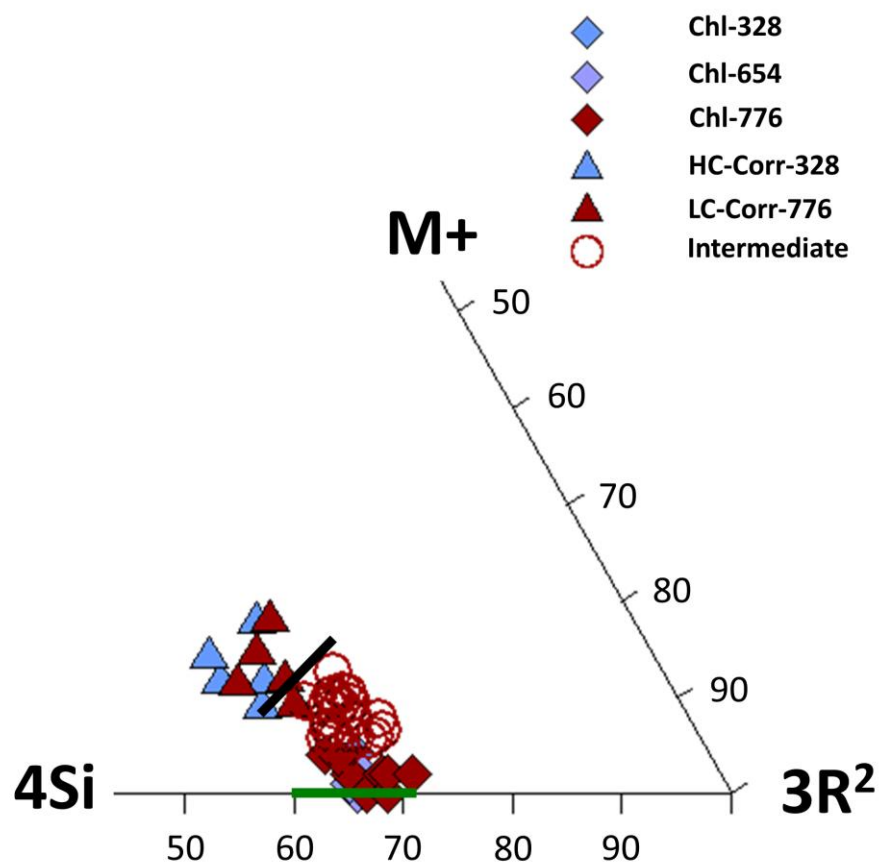
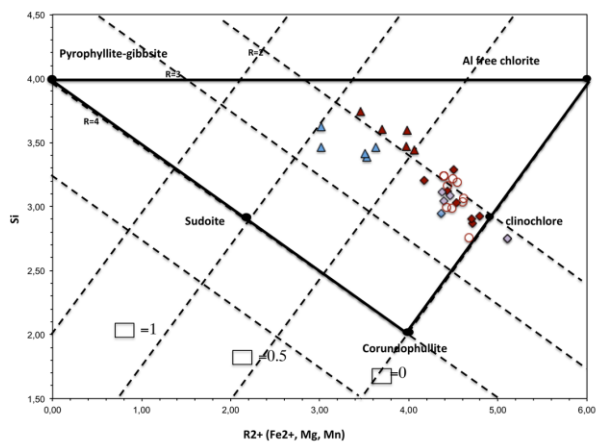


Figure 12



◆ Chl-328    ▲ HC-Corr    ◆ Chl-654    ◆ Chl-776    ▲ LC-Corr    ○ Intermediate

Fig. 13.

Table 1. Representative AEM analyses of smectites, illites and I/S mixed-layers normalized to O<sub>10</sub>(OH)<sub>2</sub>

	Si	<sup>IV</sup> Al	<sup>VI</sup> Al	Fe	Mg	Σ <sup>VI</sup>	Na	K	Ca	Σinter.
158-1	3.97	0.03	1.01	0.66	0.42	2.08	-	0.09	0.10	0.29
158-2	3.81	0.19	0.79	0.90	0.38	2.08	-	0.09	0.14	0.36
158-3	4.05	0.00	1.00	0.64	0.36	1.99	-	0.00	0.09	0.17
158-5	3.97	0.03	1.01	0.71	0.24	1.96	-	0.07	0.19	0.45
158-8	3.97	0.03	1.01	0.67	0.43	2.11	-	0.03	0.07	0.17
158-11	3.91	0.09	0.91	0.84	0.33	2.09	-	0.05	0.05	0.16
158-12	3.88	0.12	0.88	0.80	0.40	2.08	-	0.07	0.12	0.31
158-13	4.04	0.00	1.05	0.62	0.31	1.97	-	0.05	0.10	0.26
158-14	3.90	0.10	0.98	0.64	0.47	2.09	-	0.09	0.14	0.36
158-15	4.05	0.00	1.01	0.60	0.33	1.94	-	0.03	0.14	0.31
158-16	4.02	0.00	0.85	0.69	0.50	2.04	-	0.05	0.12	0.29
158-19	3.89	0.11	0.96	0.71	0.40	2.06	-	0.05	0.14	0.33
158-20	3.82	0.18	0.82	0.86	0.46	2.14	-	0.02	0.09	0.19
328-2	3.36	0.64	1.45	0.28	0.41	2.14	-	0.51	0.05	0.62
328-3	3.37	0.63	1.58	0.21	0.30	2.10	-	0.55	0.05	0.66
328-4	3.46	0.54	1.58	0.21	0.28	2.07	-	0.49	0.07	0.63
328-5	3.38	0.62	1.47	0.30	0.39	2.15	-	0.41	0.07	0.55
328-6	3.32	0.68	1.65	0.24	0.17	2.07	-	0.31	0.12	0.56
328-7	3.53	0.47	1.69	0.16	0.23	2.07	-	0.33	0.03	0.40
328-8	3.49	0.51	1.45	0.25	0.33	2.03	-	0.46	0.11	0.67
328-22	3.47	0.53	1.61	0.21	0.28	2.09	-	0.33	0.05	0.44
328-23	3.46	0.54	1.66	0.17	0.26	2.09	-	0.37	0.03	0.44
328-26	3.54	0.46	1.64	0.17	0.31	2.13	-	0.28	0.05	0.38
328-28	3.51	0.49	1.70	0.16	0.26	2.11	-	0.24	0.07	0.38
328-29	3.60	0.40	1.64	0.19	0.21	2.04	-	0.31	0.07	0.45
328-30	3.50	0.50	1.59	0.24	0.31	2.14	-	0.28	0.02	0.31
328-1A	3.72	0.28	1.71	0.14	0.21	2.06	0.00	0.21	0.10	0.41
328-2A	3.93	0.07	1.81	0.00	0.19	2.00	0.00	0.09	0.09	0.26
328-3A	3.69	0.31	1.72	0.00	0.34	2.06	0.00	0.21	0.11	0.42
328-4A	3.67	0.33	1.78	0.00	0.27	2.05	0.00	0.25	0.07	0.39
328-5A	3.77	0.23	1.67	0.19	0.26	2.12	0.00	0.21	0.07	0.34
328-6A	3.49	0.51	1.53	0.25	0.29	2.06	0.12	0.62	0.04	0.81
328-7A	3.66	0.34	1.67	0.21	0.19	2.08	0.00	0.35	0.07	0.49
328-8A	3.67	0.33	1.57	0.19	0.26	2.02	0.10	0.38	0.09	0.66
653-2	3.20	0.80	1.78	0.14	0.13	2.05	-	0.83	0.07	0.96
653-3	3.48	0.52	1.90	0.00	0.11	2.01	-	0.71	0.00	0.71
653-5	3.62	0.38	1.49	0.36	0.31	2.15	-	0.59	0.09	0.75
653-6	3.53	0.47	1.38	0.44	0.27	2.09	-	0.59	0.12	0.82
653-8	3.49	0.51	1.67	0.23	0.25	2.15	-	0.53	0.02	0.56
653-9	3.52	0.48	1.70	0.25	0.25	2.20	-	0.44	0.05	0.54
653-11	3.35	0.65	1.83	0.13	0.05	2.01	-	0.79	0.04	0.85
653-12	3.31	0.69	1.80	0.19	0.11	2.10	-	0.64	0.00	0.63
653-14	3.35	0.65	1.85	0.00	0.27	2.13	-	0.89	0.00	0.88
653-16	3.28	0.72	1.88	0.11	0.11	2.09	-	0.57	0.02	0.60
653-30	3.62	0.38	1.72	0.14	0.21	2.07	-	0.44	0.03	0.51
653-31	3.65	0.35	1.43	0.42	0.33	2.18	-	0.46	0.00	0.45
653-32	3.50	0.50	1.50	0.35	0.21	2.07	-	0.76	0.05	0.86
653-33	3.46	0.54	1.78	0.14	0.19	2.12	-	0.37	0.05	0.47
653-1A	3.33	0.67	1.77	0.07	0.12	1.96	0.39	0.30	0.11	0.90
653-2A	3.38	0.62	1.75	0.07	0.12	1.95	0.37	0.32	0.11	0.90
653-3A	3.26	0.74	1.83	0.09	0.11	2.02	0.23	0.44	0.04	0.74
653-4A	3.85	0.15	1.88	0.07	0.07	2.02	0.00	0.12	0.05	0.22
653-5A	3.52	0.48	1.87	0.11	0.07	2.05	0.18	0.19	0.04	0.44

Table 2. Representative AEM analyses of chloritic phases normalized to  $O_{10}(OH)_8$ 

	Si	<sup>IV</sup> Al	<sup>VI</sup> Al	Fe	Mg	Mn	$\Sigma^{VI}$	K	Na	Ca	$\Sigma_{inter.}$
653-17*	3.08	0.92	1.33	1.70	2.77	-	5.80	0.07	-	0.00	0.07
653-18*	3.04	0.96	1.39	1.50	2.90	-	5.78	0.00	-	0.00	0.00
653-22**	3.17	0.83	1.39	1.77	2.55	-	5.72	0.00	-	0.07	0.14
653-6A**	2.87	1.13	1.67	2.32	1.74	-	5.73	0.03	0.20	0.00	0.23
653-8A**	2.99	1.01	1.43	2.80	1.57	-	5.79	0.07	0.00	0.10	0.27
653-9A**	3.12	0.88	1.38	2.09	2.28	-	5.75	0.02	0.00	0.00	0.02
653-10A**	2.92	1.08	1.65	2.56	1.51	-	5.72	0.10	0.00	0.00	0.10
653-13A**	3.09	0.91	1.04	2.12	2.77	-	5.94	0.00	0.00	0.07	0.14
653-14A*	2.75	1.25	1.01	2.31	2.80	-	6.12	0.00	0.00	0.02	0.05
776-1**	3.07	0.93	1.24	2.27	2.34	-	5.85	0.05	-	0.10	0.24
776-2*	3.12	0.88	1.34	2.19	2.24	-	5.77	0.00	-	0.02	0.05
776-3*	3.20	0.80	1.48	1.92	2.25	-	5.66	0.00	-	0.05	0.09
776-4**	3.04	0.96	1.25	2.29	2.31	-	5.86	0.00	-	0.12	0.24
776-5**	3.19	0.81	1.24	2.30	2.25	-	5.78	0.10	-	0.12	0.34
776-6**	3.22	0.78	1.26	2.02	2.48	-	5.76	0.02	-	0.12	0.26
776-7**	3.07	0.93	1.23	2.23	2.38	-	5.85	0.05	-	0.05	0.14
776-9**	2.99	1.01	1.35	2.27	2.22	-	5.83	0.07	-	0.10	0.27
776-10**	2.85	1.15	1.29	2.17	2.46	-	5.93	0.00	-	0.07	0.14
776-11*	3.03	0.97	1.30	2.20	2.34	-	5.83	0.00	-	0.00	0.00
776-12*	2.90	1.10	1.23	2.14	2.57	-	5.93	0.00	-	0.02	0.05
776-13**	2.99	1.01	1.38	1.89	2.54	-	5.81	0.05	-	0.05	0.14
776-14*	2.93	1.07	1.16	2.16	2.64	-	5.96	0.00	-	0.00	0.00
776-15**	3.16	0.84	1.32	2.25	2.18	-	5.76	0.07	-	0.07	0.22
776-16**	2.76	1.24	1.30	2.13	2.54	-	5.97	0.05	-	0.07	0.19
776-17*	3.29	0.71	1.24	2.17	2.33	-	5.74	0.00	-	0.05	0.10
776-18**	3.24	0.76	1.33	2.04	2.35	-	5.72	0.05	-	0.10	0.24
776-20**	3.24	0.76	1.33	2.04	2.35	-	5.72	0.05	-	0.10	0.24
776-2A**	3.20	0.80	1.40	2.25	2.05	-	5.70	0.02	0.00	0.07	0.17
776-4A**	3.02	0.98	1.30	2.10	2.44	-	5.84	0.00	0.00	0.10	0.19
776-5A**	3.21	0.79	1.29	2.37	2.10	-	5.75	0.02	0.00	0.12	0.27
776-6A**	3.20	0.80	1.41	2.24	2.04	-	5.69	0.00	0.00	0.10	0.19
776-7A**	3.32	0.68	1.31	2.06	2.32	-	5.68	0.00	0.00	0.07	0.14
776-8A**	3.43	0.57	1.39	2.06	2.13	-	5.59	0.00	0.00	0.12	0.24
776-10A**	3.25	0.75	1.26	2.34	2.08	0.07	5.75	0.00	0.00	0.07	0.14
776-11A**	2.93	1.07	1.05	2.66	2.22	0.07	6.01	0.02	0.00	0.07	0.17
776-12A*	2.87	1.13	1.20	2.60	2.12	0.05	5.97	0.00	0.00	0.02	0.05
776-17A**	3.20	0.80	1.20	2.24	2.31	0.05	5.80	0.00	0.00	0.07	0.14
776-13A**	3.09	0.91	1.04	2.12	2.77	-	5.94	0.00	0.00	0.02	0.05
776-14A**	2.75	1.25	1.01	2.31	2.80	-	6.12	0.00	0.00	0.60	1.20
776-17A**	3.20	0.80	1.08	2.38	2.41	-	5.86	0.07	0.00	0.07	0.22
328-15*	2.95	1.05	1.44	2.13	2.23	-	5.80	0.05	0.00	0.02	0.10

\*Chlorites; \*\*Chlorites mixed layer

Table 3. Representative AEM analyses of corrensites normalized  $O_{20}(OH)_{10}$ 

	Si	<sup>IV</sup> Al	<sup>VI</sup> Al	Fe	Mg	Mn	$\Sigma^{VI}$	K	Ca	$\Sigma$ inter.
328-12	6,18	1,82	3,02	2,57	2,82	-	8,40	0,29	0,08	0,46
328-14	6,04	1,96	2,45	3,26	3,04	-	8,75	0,21	0,30	0,81
328-16	6,09	1,91	2,46	3,03	3,24	-	8,72	0,13	0,13	0,38
328-19	6,47	1,53	2,92	2,61	2,77	-	8,30	0,34	0,13	0,59
328-20	6,18	1,82	2,29	3,09	3,39	-	8,77	0,17	0,17	0,51
776-8	6,19	1,81	1,88	3,31	3,77	-	8,96	0,13	0,21	0,55
775-1A	6,14	1,86	1,79	3,52	3,73	-	9,03	-	0,21	0,42
776-3A	6,44	1,56	2,12	3,51	3,09	-	8,72	-	0,34	0,68
776-9A	6,69	1,31	2,26	3,15	3,03	0,08	8,53	-	0,25	0,50
776-13A	6,42	1,58	1,79	3,34	3,76	-	8,89	0,04	0,43	0,90

**Highlights**

We present HRTEM data from 900 m of drill core for the first time in active Chilean geothermal field

There is concordance between present day measured temperatures and clay mineral association

We found also strong textural and chemical characteristics of non-equilibrium mineral features

HRTEM work is important to understand the alteration processes in active geothermal systems

ACCEPTED MANUSCRIPT